RBM7 deficiency promotes breast cancer metastasis by coordinating MFGE8 splicing switch and NF-kB pathway

Fang Huang[1†], Zhenwei Dai[1†], Jinmiao Yu[1†], Kainan Wang[†2], Chaoqun Chen[1], Dan Chen[3], Jinrui Zhang[4], Jinyao Zhao[4], Mei Li[4], Jinyao Zhao[4], Wenjing Zhang[4], Xiaojie Li[5*], Yangfan Qi[4,6*], Yang Wang[1*]

[1]Sino-US Research Center for Cancer Translational Medicine of the Second Affiliated Hospital of Dalian Medical University & Institute of Cancer Stem Cell, Dalian Medical University, Dalian 116023, China

[2]Department of Oncology & Sino-US Research Center for Cancer Translational Medicine, the Second Affiliated Hospital, Dalian Medical University, Dalian 116023, China

[3]Department of Pathology, the First Affiliated Hospital of Dalian Medical University, Dalian Medical University, Dalian 116011, China

[4]Institute of Cancer Stem Cell, Dalian Medical University, Dalian 116044, China

[5]Department of Prosthodontics, College of Stomatology, Dalian Medical University, Dalian, 116044, China.

[6]Soochow University Cancer Institute, Suzhou, China

[†] These authors contributed equally to this work.

[*] Correspondence:

21 Yang Wang; Sino-US Research Center for Cancer Translational Medicine of the
22 Second Affiliated Hospital of Dalian Medical University & Institute of Cancer Stem
23 Cell, Dalian Medical University, Dalian 116023, China; Tel: +86-411-86110531;
24 Email: yangwang@dmu.edu.cn

25 Yangfan Qi; Institute of Cancer Stem Cell, Dalian Medical University, Dalian, China
26 116044; Tel: +86-411-86110531; Email: yangfanqi@dmu.edu.cn

27

28

29 Running title: RBM7 presents anti-metastasis activity by regulating splicing

30

31

32 We declare no conflict of interest on the studies described in this manuscript.

Abstract

Aberrant alternative splicing is well-known to be closely associated with tumorigenesis of various cancers. However, the intricate mechanisms underlying breast cancer metastasis driven by deregulated splicing events remain largely unexplored. Here, we unveiled that RBM7 is decreased in lymph node and distant organ metastases of breast cancer as compared to primary lesions and low expression of RBM7 is correlated with the reduced disease-free survival of breast cancer patients. Breast cancer cells with RBM7 depletion exhibited an increased potential for lung metastasis compared to scramble control cells. The absence of RBM7 stimulated breast cancer cell migration, invasion, and angiogenesis. Mechanistically, RBM7 controlled the splicing switch of MFGE8, favoring the production of the predominant isoform of MFGE8, MFGE8-L. This resulted in the attenuation of STAT1 phosphorylation and alterations in cell adhesion molecules. MFGE8-L exerted an inhibitory effect on the migratory and invasive capability of breast cancer cells, while the truncated isoform MFGE8-S, which lack the second F5/8 type C domain had the opposite effect. In addition, RBM7 negatively regulates the NF-κB cascade and an NF-κB inhibitor could obstruct the increase in HUVEC tube formation caused by RBM7 silencing. Clinically, we noticed a positive correlation between RBM7 expression and MFGE8 exon7 inclusion in breast cancer tissues, providing new mechanistic insights for molecular-targeted therapy in combating breast cancer.

Keywords: RBM7; alternative splicing; breast cancer; metastasis

Introduction

Alternative splicing (AS) emerges as a substantial contributor to the production of a myriad of transcripts from limited genes, which enriched protein variation and phenotypic diversity in multicellular organisms. Pre-mRNA splicing reactions require a step-wise assembly of spliceosome, a megadalton complex that recognize consensus regulatory sequences, including 5' and 3' splice sites marking exon-intron boundary, and the branch point site (BPS), to accomplish exon definition (Shi, 2017) (Wilkinson, Charenton et al., 2020). While a splice site is suboptimal, AS emerges under control of inherent sequence acting in cis, namely exonic or intronic splicing enhancer or silence, and the cognate trans-acting splicing factors, which can strengthen or weaken the recognition of splice sites by spliceosome.

It is well documented that AS dysregulation leads to multiple human diseases, including cancer (Montes, Sanford et al., 2019) (Singh & Cooper, 2012). Tumorigenicity has been linked with cancer-specific splicing switch arising from either cis-elements mutations or deregulated splicing regulatory factors. In some cases, splicing factors, particularly spliceosomal components SF3B1 and U2AF1, are frequently mutated across diverse cancer types (Baralle, 2005) (Harbour, Roberson et al., 2013) (Smith, Choudhary et al., 2019) (Cheruiyot, Li et al., 2021). For instance, recurrent SF3B1 mutations led to retention of intronic region in BRD9 pre-mRNA, conferring loss of core subunit function to the ncBAF chromatin remodeling complex and metastatic advantage to melanoma cells (Inoue, Chew et al., 2019). Another layer of regulation involves the abnormal expression of splicing factors derived from

77 altered regulatory pathway. As an archetypal example, a set of members in SR protein
78 family such as SRSF1 and SRSF3 are upregulated in breast tumors, lung tumors,
79 glioma and exhibit oncogenic ability via altering AS products (for example, Bcl-x,
80 MYO1B, NUMB and p53) (Anczuków, Akerman et al., 2015) (Zhou, Wang et al.,
81 2019) (Tang, Horikawa et al., 2012) (Zhou, Gong et al., 2020). Otherwise, many
82 splicing factors such as RBM (RNA binding motif) proteins can either functions as
83 oncoproteins or tumor suppressors in cancer-type dependent manner (Li, Guo et al.,
84 2021), which may be attributed to tissue-specific AS patterns.

85 Breast cancer is the most common diagnosed malignancy and remain the second
86 leading cause of cancer mortality (over 41,000 deaths annually in the USA) among
87 females worldwide (Siegel, Miller et al., 2019). Metastasis to vital organs accounts for
88 approximately 90% cancer-related death. The 5-year overall survival rate of patients
89 with metastatic breast cancer is drastically decreased to about 25%, as compared to
90 the primary cancer patients' prognosis with a survival rate greater than 80% (Rabbani
91 & Mazar, 2007) (Valastyan & Weinberg, 2011). Despite advances in early diagnosis
92 and comprehensive interventions for breast cancer treatment, limited effective
93 strategy against metastasis has been an outstanding challenge for improving
94 prognostication of patients. This highlights the urgent need for deepened
95 understanding of mechanisms underlying development of metastasis. Tumor
96 metastasis is multi-step process involving a sequential cascade of events, such as
97 epithelial-mesenchymal transition (EMT), local invasion from primary tumor site,
98 lymphogenic or hematogenic dissemination, cancer cells seeding and metastatic

99 lesions formation (Liang, Zhang et al., 2020). AS dysregulation has been implicated in
100 multistage process of metastasis. For example, the switch of CD44 or FGFR2 splicing
101 isoforms can lead to EMT phenotype (Chen, Zhao et al., 2018) (Warzecha, Sato et al.,
102 2009). VEGF-A or XBP1 splicing transition is tightly linked to angiogenesis in cancer
103 (Bates, 2008) (Zeng, Xiao et al., 2013). On account of the phenotypic plasticity in
104 metastatic cells conferred by alternative splicing, further investigation in potential role
105 of critical splicing regulatory factors and the associated splicing events in breast
106 cancer metastasis is warranted.

107 RNA-binding proteins (RBPs) are a large class of conserved proteins that
108 participate in cancer development through precisely control RNA metabolism,
109 including RNA splicing. RBM7, a member of RBP family, is commonly known to
110 exert RNA surveillance activity as a component of the human nuclear exosome target
111 (NEXT) complex (Meola, Domanski et al., 2016) . Aberrant expression of RBM7 is
112 not only associated with lung fibrosis onset and motor neuronopathy, but also impacts
113 cancer cell proliferation (Fukushima, Satoh et al., 2020) (Xi, Zhang et al., 2020).
114 Previous findings have established a direct connection of RBM7 with spliceosome
115 factors SF3B2 and SF3B4 (Falk, Finogenova et al., 2016), yet whether RBM7 is
116 involved in the regulation of AS remain elusive. In this study, we report that RBM7 is
117 frequently reduced in a subset of breast cancer metastases from lymph nodes lesions
118 and distant organ as compared to primary tumors and its low expression predicts
119 dismal survival outcomes of patients. Breast cancer cells with loss of RBM7 gain
120 enhanced aggressive capability and metastatic potential. Mechanistically, RBM7

121 ablation enhanced the splicing switch of MFGE8 pre-mRNA from canonical isoform
122 MFGE8-L to a truncated isoform MFGE8-S. Ectopic expression of MFGE8-L caused
123 marked suppression of migratory and invasive ability of breast cancer cells, whereas
124 MFGE8-S showed opposite function/ disabled such function. At another layer, RBM7
125 discordantly regulated the phosphorylation of p65. In concert, NF-κB inhibitor
126 abolished pro-angiogenesis effect of RBM7 ablation in breast cancer. Above all, our
127 findings uncovered a previously unidentified role of RBM7 in breast cancer
128 metastasis via coupling MFGE8 splicing switch and NF-κB signaling activation,
129 suggesting a new therapeutic target and prognostic predictor for breast cancer.

130 **Results**

131 **RBM7 is reduced in metastatic lesions of breast cancer and positively correlated**

132 **with patients' prognosis**

133 To determine the clinical relevance of RBM7 in breast cancer, we assessed the

134 correlation between RBM7 and important clinical outcomes. Analysis of TCGA, GEO

135 and the METABRIC breast cancer datasets showed that RBM7 expression positively

136 correlates with overall survival of breast cancer patients (Figure 1A and

137 Supplementary Figure 1A-1B). RBM7 low expression predicts the reduced

138 disease-free survival in patients with breast cancer (Figure 1B and Supplementary

139 Figure 1C). Congruently, we found RBM7 is decreased in breast cancer compared to

140 normal tissues (Figure 1C and Supplementary Figure 1D). Further dissection in a

141 cohort of breast cancer patients from the cBioPortal unveiled cases with lymph node

142 metastasis have lower expression of RBM7 as compared to cases without metastasis

143 (Figure 1D). We next performed immunohistochemistry (IHC) detection of RBM7 in

144 breast cancer tissue microarrays. The results showed that patients bearing clinical

145 stage III tumors have significantly decreased RBM7 expression than patients bearing I

146 and II clinical stage tumors (Figure 1E). In tissue chip containing triple negative

147 breast cancer, the more aggressive and mesenchymal breast cancer subtype, RBM7

148 exhibits reduced protein levels in tumors as compared to paracancer tissues (Figure

149 1F). In addition, we collect specimen consisted of tumor tissues from 21 breast

150 primary cancer, in 9 cases, from metastatic loci and took advantage of IHC analysis to

151 determine the RBM7 expression. Most (25% strong positive;67% moderate positive)

152 of primary tumor samples displayed a positive IHC staining for RBM7, whereas most
153 of lung/liver metastatic lesions showed weak or negative RBM7 expression (Figure
154 1G). We also obtained paired primary breast cancer and lymph node metastatic loci
155 and found, when compared to the corresponding primary tumor, the expression of
156 RBM7 is significantly decreased in lymph node metastases (Figure 1H-1I). These
157 results associated RBM7 with breast cancer metastasis, prompting us to further
158 investigate the functional role of RBM7 in metastatic processes of breast cancer.
159

160 **RBM7 silencing provokes metastatic potential of breast cancer**

161 In light with the above findings, we generated RBM7-silenced breast cancer cells
162 using lentiviral expression of short hairpin RNA (shRNA) followed by profiling
163 high-throughput transcriptome by RNA sequencing. Strikingly, Gene Ontology and
164 pathway analysis displayed a wide range of differentially expressed genes were
165 enriched in extracellular matrix organization, cell migration and angiogenesis (Figure
166 2A-2B), which have been characterized as crucial processes in tumor metastasis. We
167 then conducted qRT-PCR analysis of theses metastasis-associated genes in
168 RBM7-depleted breast cancer cells and verified that they were up-regulated upon
169 RBM7 knockdown shown as heatmap representation (Figure 2C). The lung metastasis
170 is one of the most prevalent distant metastases that breast cancer is prone to and
171 associated with poor prognosis of patients (Medeiros & Allan, 2019). Thus, we
172 performed tail-vein transfer model to evaluate the potential impact of RBM7 on
173 pulmonary metastasis of breast cancer cells. 6×10^5 4T1 cells, the mouse breast cancer

174 cell line simulating stage IV human breast tumor, with stable RBM7 silence or control
175 vector were implanted into BALB/c mice via tail vein. RBM7-silenced 4T1 cells were
176 able to develop more spontaneous lung metastases than control cells as judged by
177 pulmonary nodules number and haematoxylin-eosin (HE) staining of lung tissues
178 (Figure 2D-2F and Supplementary Figure 2A). Cancer metastasis is comprised of a
179 complex cascade of events, such as migration, invasion and angiogenesis, thus we
180 next to determine which process is mediated by RBM7-loss in facilitating breast
181 cancer metastasis. We utilized transwell chamber with or without matrix coat and
182 would healing assays to examine the potential function of RBM7 in migration and
183 invasion capabilities and found the depletion of RBM7 led to a visible increase in
184 mobility and invasiveness of both the triple-negative breast cancer (TNBC) cell line
185 MDA-MB-231, estrogen receptor positive breast cancer cell line MCF7 and 4T1 cells
186 (Figure 2G-2H and Supplementary Figure 2B-2E). Conversely, RBM7 overexpression
187 notably repressed MDA-MB-231 and MCF7 cells to migrate or invade across
188 transwell inserts (Figure 2I-2J). Similar results were obtained in two additional TNBC
189 cell lines BT549 and HCC1937 (Supplementary Figure 2F-2G), which proved that
190 RBM7 possessed the capability to suppress the migration and invasion of breast
191 cancer cells. To examine the impact of RBM7 on angiogenesis in breast cancer, we
192 cultured human umbilical vein endothelia cells (HUVEC) with condition medium
193 obtained from culture supernatants of RBM7-depleted or scramble shRNA transduced
194 cells for tube formation analysis. Compared to the scramble control, HUVEC
195 incubated with culture medium from RBM7-knockdown breast cancer cells exhibited

196 accelerated tube formation length and branch junction (Figure 2K), suggesting the
197 inhibitory effect of RBM7 on breast cancer angiogenesis. Taken together, the above
198 data demonstrated RBM7 as tumor suppressor by regulating breast cancer migration,
199 invasion and angiogenesis.
200

201 **RBM7 exhibits splicing regulatory function in breast cancer**

202 In previous studies, RBM7 is commonly characterized as an RNA-binding
203 constituent of trimeric NEXT complex, which directs the RNA exosome to
204 non-coding transcriptome for degradation (Lubas, Andersen et al., 2015). However,
205 the mechanistical role of RBM7 in cancer remain largely unknown. Intriguingly, we
206 observed that, attributed to the ablation of RBM7, almost 551 splicing events occurred
207 significant decrease in PSI (percent spliced in), whereas 289 splicing events endured
208 increased PSI (Figure 3A). The changed events were divided among various types of
209 AS (alternative splicing), including SE (skipping exon), IR (intron retention), A5E
210 (alternative 5' splice site exon), A3E (alternative 3' splice site exon), and MXE
211 (mutually exclusive exons), of note, SE events were the most prominently regulated
212 (Figure 3B). A majority of AS events in particular of SE and A5E category were in
213 decrease of PSI upon RBM7 depletion (Figure 3C-3D), indicating that the presence of
214 RBM7 may promote the usage of alternative splice sites of SEs or A5Es.
215 Subsequently, we extracted the candidate binding motifs which reside within or near
216 cassette exons or A5E and found UUUCUU motif, simiar to RBM7 binding site
217 (polyU) were enriched in RBM7 positively regulated AS events to a greater extent

218 that control exons unimpacted by RBM7 (Figure 3E), raising the possibility that
219 RBM7 may serve as a splicing activator through directly tethering cis-element in
220 pre-mRNA. This is coherent with the nuclear localization of RBM7 in breast cancer
221 cells (Supplementary Figure 3A). In order to explore the splicing regulation activity
222 of RBM7 in distinct pre-mRNA context, we validated a series of
223 RBM7-significantly-changed splicing events across different AS types according to
224 the RNA-seq results. The RT-PCR analysis demonstrated that the PSI of selected gene
225 related to cancer progression was either increased or decreased endogenously upon
226 RBM7 depletion (Figure 3F and Supplementary Figure 3B). Considering that the AS
227 is a sophisticated multi-step reaction that is regulated by both pre-mRNA-interacting
228 splicing factor and other assistant factors in a context-dependent manner (Wright,
229 Smith et al., 2022), we doubted the divergent effect of RBM7 on distinct splicing
230 targets was due to a more complicated mechanism. Gene ontology (GO) enrichment
231 analysis identified a majority of genes undergoing AS alterations were involved in
232 cytoskeleton assembly and organization (Figure 3G). While globally analyzing the
233 network enrichment of RBM7-regulated downstream splicing events, we observed its
234 targets are functionally connected to well-linked network containing gene subgroups
235 (Figure 3H), which are associated with biological processes in tumor cell metastasis,
236 again suggesting the cancer-related function of RBM7.
237
238 **RBM7 depletion switches splicing outcomes of MFGE8 by decreasing MFGE8-L**
239 **isoform**

240 To ascertain the functional targets that explain the inhibitory role of RBM7 in
241 breast cancer metastasis, we analyzed RNA immunoprecipitation sequencing data for
242 RBM7 and whole-transcriptome sequencing data for breast cancer cells expressing
243 two shRNAs targeting RBM7. Venn diagram of 8 hub genes obtained by overlapping
244 three gene sets pointed forward a hotspot gene, namely MFGE8 (Figure 4A).
245 RNA-seq data showed that the depletion of RBM7 resulted in a significant alteration
246 in ratio of MFGE8 two isoforms, of which the canonical isoform (MFGE8-L) has
247 been demonstrated to be correlated with tumor formation and aggressiveness of breast
248 cancer (Yang, Hayashida et al., 2011). Importantly, the exon 7 located in F5/8 type C
249 2 domain, which is obligated to bind to phosphatidylserine, was lacked in the short
250 isoform of MFGE8 (MFGE8-S) (Figure 4B). Further RT-PCR identification verified
251 RBM7 ablation indeed potentiated the production of MFGE8-S in various TNBC cell
252 lines (Figure 4C). Similar results were obtained from MCF7 cells, suggesting that
253 RBM7 regulated the AS of MFGE8 independently of the ER status. In separate
254 experiments, we transfected breast cancer cells with an exogenous MFGE8 splicing
255 reporter containing exon 6-8 and 600bp of flanking intron sequences to determine the
256 splicing regulatory function of RBM7. Accordingly, the depletion of RBM7 still
257 induced the splicing shift of the minigene reporter by elevating MFGE8-S variant
258 (Figure 4D). To test whether such splicing regulatory effect was directly or indirectly,
259 we analyzed the sequence of alternative exon 7 and the motifs nearby its 5' or 3'
260 splice sites, and found two poly(U) motifs are positioned in proximal to the pseudo 3'
261 splice site. Subsequent RT-PCR assay for the precipitation in RIP assays confirmed

262 RBM7 could bind to the upstream sequence containing UUUCUU motifs adjacent to
263 3' splice site of MFGE8 cassette exon, but not another region nearby it (Figure 4E).
264 To pinpoint the location for the potential cis-element for AS regulation by RBM7, we
265 designed antisense oligonucleotides (ASOs), which have been chemically modified to
266 avoid endogenous nuclease degradation without recruiting RNase H, to block the
267 UUUCUU residues in proximity to intron6/exon7 junction. As shown in Figure 4F,
268 when compared to control ASO, treatment with ASOs targeting the potential binding
269 site (UUUCUU) of RBM7, contributed to the exclusion of exon7 of MFGE8. In
270 separate experiments, the depletion of RBM7 induced the splicing shift of the
271 minigene reporter by elevating MFGE8-S variant. While the binding motif was
272 depleted or mutated, RBM7 failed to affect the splicing outcomes of MFGE8
273 (Supplementary Figure SC). Due to its close proximity to 3' splice site, UUUCUU
274 residues bound by RBM7 might participated in spliceosome assembly on the
275 upstream 3' splice site of exon7, which may explain why disruption of the motif led
276 to almost complete exon7 skipping. Oue data suggest that RBM7 regulates the exon
277 skipping of MFGE8 by directly binding to UUUCUU located at six nucleotides
278 upstream of the 3' splice-site of exon7.
279

280 **The short variant of MFGE8 abolishes the inhibitory function of its classical**
281 **isoform on breast cancer cell migration and invasion**

282 MFGE8 encodes a secreted protein, Milk fat globule-EGF factor 8 (MFG-E8),
283 which participates in a variety of cellular processes, including mammary gland

284 branching morphogenesis, angiogenesis and mucosal healing, etc (Raymond, Ensslin
285 et al., 2009). We applied MFGE8-L stably overexpressing- or depleted-breast cancer
286 cells to transwell assays and observed the cellular migratory and invasive capabilities
287 was visibly suppressed by MFGE8-L overexpression (Supplementary Figure 4A-4B).
288 On the contrary, the knockdown of MFGE8-L provoked cell migration and invasion
289 (Supplementary Figure 4C). Strikingly, while MDA-MB-231 or HCC1937 expressing
290 MFGE8-L showed a remarkable decrease in migratory and invasive ability compared
291 to control vector, MFGE8-S not only totally abolished the inhibitory function of
292 MFGE8-L but elicited modest pro-migration/ invasion actions on breast cancer cells
293 (Figure 5A and Supplementary Figure 4D-4E). We also performed Fluorescent
294 Gelatin Degradation Assays for investigating invadopodia formation and found
295 MFGE8-L up-regulation suppressed breast cancer cells invasion through a layer of
296 extracellular matrix, whereas breast cancer cells with ectopic expression of MFGE8-S
297 acquired enhanced ability to degrade matrix and invasion (Figure 5B).
298 Immunofluorescence assays revealed the MFGE8-L forms foci in cytoplasm,
299 particularly enriched near cell-cell contact sites, whereas MFGE8-S is more evenly
300 distributed in the nucleus and cytoplasm (Figure 5C). As shown in diagram of domain
301 configuration for two variants, in comparison with MFGE8-L isoform containing
302 N-terminal EGF-like domain and C-terminal twice-repeated F5/8 type C domains, the
303 protein encoded by MFGE8-S loses the second F5/8 type C domain, implying a
304 shortage of the function corresponding to membrane-binding (Supplementary Figure
305 4F). The different structural bases of two isoforms may also be linked to their distinct

306 cellular function in tumor invasion (Supplementary Figure 4G). Furthermore, we
307 compared transcriptome profiles between MFGE8-L and MFGE8-S ectopically
308 expressing breast cells and found a set of functional genes were down-regulated by
309 MFGE8-L, whereas this negative regulation was abrogated in response to MFGE8-S
310 (Supplementary Figure 4H). The differentially expressed genes between two splice
311 variants were predominantly enriched in cell adhesion molecules and JAK-STAT
312 cascade as revealed by KEGG pathway and Gene ontology analysis (Figure 5D and
313 Figure 5E). Subsequent experimental validation demonstrated that the activation of
314 STAT1 was hindered by MFGE8-L, but not affected by MFGE8-S (Figure 5F).
315 Considering that STAT1 signaling activation plays an important role in tumor cell
316 metastasis via cell adhesion molecules induction (Marimuthu, Lakshmanan et al.,
317 2022) (Chen, Hao et al., 2019), it is highly plausible that MFGE8-L, but not
318 MFGE8-S, impeded breast cancer cell motility and invasive capability in a
319 STAT1-dependent manner.
320

321 **RBM7 depletion-stimulated aggressiveness of breast cancer is dependent on**
322 **MFGE8 splicing switch and NF-kB pathway activation**

323 Next, we sought to assess if MFGE8 splicing switch is responsible for
324 acquisition of aggressive feature in RBM7-silenced breast cancer cells. Flag-tagged
325 MFGE8-L or an empty vector was co-expressed in MDA-MB-231 cells together with
326 RBM7 shRNA (Supplementary Figure 5A). Following seeding into transwell chamber,
327 cells transfected with RBM7 shRNA exerted a higher migratory and invasive

328 capability than scramble control, consistent with above data. Importantly, the
329 restoration of MFGE8-L expression diminished the acquired aggressive properties of
330 MDA-MB-231 cells resulted from RBM7 depletion (Figure 6A). Similar results were
331 obtained using RBM7-depleted MCF7 cells with or without MFGE8-L complement
332 (Figure 6A). To corroborate the role of MFGE8 splicing shift in RBM7- regulated
333 breast cancer cell invasion, we transfected triple-negative breast cancer cells with
334 ASOs directed against RBM7-binding motif and examined the potential impact on
335 cell aggressiveness. The results showed an obvious increase in exon7-skipped variant
336 as compared to the scramble negative control ASOs (Supplementary Figure 5B).
337 Meanwhile, the migrative and invasive ability of breast cancer cells treated with
338 ASOs was significantly boosted (Figure 6B), further suggesting that
339 RBM7-knockdown stimulated aggressiveness of breast cancer at least partially relies
340 on the control of MFGE8 AS. However, a series of shRBM7-upregulated secreted
341 factors that have been reported to drive tumor angiogenesis (Gopinathan, Milagre et
342 al., 2015) (Fousek, Horn et al., 2021) (Feng, Ke et al., 2019), were not impacted by
343 MFGE8-L/S (Figure 6C and Supplementary Figure 5C). Condition medium derived
344 from breast cancer cells overexpressing MFGE8-L/S showed negligible effect on
345 HUVEC tube formation (Supplementary Figure 5D, implying that there exists
346 additional mechanism underlying breast cancer metastasis attributed to RBM7
347 reduction.

348 Given that consecutive gene set enrichment analysis (GSEA) of highest-ranking
349 gene sets based on transcriptomic profile of mRNA expression showed a signature for

350 NF-κB pathway that was augmented upon depletion of RBM7 (Figure 6D), we
351 suspected that the transcriptional activation of downstream genes in NF-κB signaling
352 known to facilitate tumor angiogenesis might be involved in shRBM7-exerted
353 pro-metastatic function. As expected, the phosphorylation of p65, a core transcription
354 factor well-known to switch on NF-κB pathway, was notably enhanced by RBM7
355 knockdown. Meanwhile, IκBα phosphorylation that can blockade p65 activation was
356 curbed upon RBM7 knockdown (Figure 6E). Conversely, RBM7 overexpression
357 impeded the activation of p65 (Supplementary Figure 5E). Yet MFGE8-L/S had no
358 effect on phosphorylation of p65 or IκBα (Supplementary Figure 5F). We found
359 RBM7 depletion remarkably promoted the expression of IL-1β as judged by qPCR
360 and ELISA assays (Supplementary Figure 5G-5I). IL-1β, commonly known as a
361 pro-inflammatory cytokine, could bind to IL-1R and initiate a multistage enzymatic
362 reaction that triggers the activation of NF-κB pathway (Weber, Kracht et al., 2010)
363 (Guo, Jin et al., 2024). Thus, it is plausible the upregulation of IL-1β might be a
364 causal factor in RBM7-depletion-induced activation of NF-kB signaling. We further
365 carried out Matrigel tube formation assays and found NF-κB inhibitor PDTC
366 drastically reversed the promotion of HUVEC angiogenesis by conditional medium
367 harvested from RBM7-depleted cells (Figure 6F-6G), implying that RBM7-p65 axis
368 may participate in HUVEC angiogenesis through reprogramming the secretome of
369 breast cancer cells. Similar effect was observed with respect to cell motility and
370 invasion (Supplementary Figure 5J). Taken together, these data above indicated that
371 both MFGE8 splice switch and NF-κB pathway activation are required for mediating

372 the pro-metastasis activity of RBM7 reduction in breast cancer.

373

374 **The PSI of MFGE8 exon 7 is decreased in breast cancer patients and positively**

375 **correlated with RBM7 expression**

376 To study the clinical relevance of MFGE8 isoform switch, we analyzed the PSI

377 changes of cassette exon7 in TCGA breast cancer cohort and found exon7 skipping

378 occurs more frequently in tumor than in normal tissues (Figure 7A). Consistently, in

379 comparison with normal counterparts, the splicing of MFGE8 is shifted towards a

380 reduced proportion of MFGE8-L across multiple cancer types, including LUAD,

381 HNSC, COAD, etc (Supplementary Figure 6A). RT-PCR assay was performed in

382 surgical tumor specimens in breast cancer patients and showed increased proportion

383 of exon7 exclusion in most tumor samples when compared to normal tissues (case#1:

384 86:94; case#2: 84:86; case#3: 79:85; case#4: 63:75; case#5: 69:93; case#6: 71:80)

385 (Figure 7B). On the other hand, the lymph node metastases contain a higher

386 proportion of MFGE8 variant with skipped exon7 in comparison with paired primary

387 tumor tissues (case#1: 80:95; case#2: 86:97; case#3: 84:90; case#4: 70:78; case#5:

388 83:89) (Figure 7C). This is coherent with decreased RBM7 expression levels found in

389 breast cancer with lymph node metastasis. In addition, patients with high expression

390 of MFGE8 exon7 had a visibly better overall survival than patients with low

391 expression (Figure 7D). We performed Pearson correlation test and revealed a

392 noticeably positive correlation between the expression of RBM7 and exon7 inclusion

393 of MFGE8 in breast cancer (Figure 7E), further supporting MFGE8 isoform switch

394 regulated by RBM7.

395

396 **Discussion**

397 Previous reports have recognized the RNA-binding protein RBM7 as a
398 component of the NEXT complex that could facilitate RNA exosome targeting to a
399 subset of non-coding RNAs and aberrant transcripts (Meola et al., 2016) (Pascal
400 Preker, 2008), including short-lived exosome substrates and pre-mRNAs, for
401 surveillance and turnover . In addition to this specific characteristic, RBM7 was
402 shown to interact with subunits of 7SK snRNP complex and thus activate P-TEF
403 downstream genes in response to DNA damage (Bugai, Quaresma et al., 2019).
404 Herein, we discover a novel role of RBM7 in alternative splicing control through
405 directly binding to its cognate cis-element in pre-mRNA. Using whole-transcriptome
406 sequencing, we found the depletion of RBM7 contributed to exon exclusion in
407 approximately 70% SE/A5E events, implying RBM7 mainly functions as a splicing
408 activator in the context of SE/A5E in breast cancer. However, the increase of PSI also
409 occurred due to RBM7 knockdown in a smaller faction of splicing events, such as
410 ZMYND8. We speculated this converse impact may be associated with the
411 intrinsically sophisticated splicing processes driven by distinct core splicing factors,
412 cognate cis-acting element and co-factors in a context-dependent manner (e.g.,
413 pre-mRNA structure, base modification, antagonistic or cooperative effect of multiple
414 splicing factors). Similar to many splicing factors, like SR proteins and hnRNPs,
415 RBM7 has an RRM-domain required for target RNA recognition in the N-terminus.

416 We performed co-IP experiment and found that RBM7 could interact with RNA
417 splicing factor SF3B2, a component of spliceosomal U2 SnRNP complex
418 (Supplementary Figure 6B). Consistent with the AS regulation of MFGE8 by RBM7,
419 the depletion of SF3B2 also promoted exon7 skipping (Supplementary Figure 6C-6D),
420 implying a cooperative effect of the two proteins in regulating MFGE8 splicing. This
421 is in concert with a previous study that RRM domain of RBM7 could bind a
422 proline-rich segment within SF3B2 (Falk, Finogenova et al., 2016). The interaction
423 mode with strong similarity to $RBM7^{RRM}$–$ZCCHC8^{Proline}$ interaction in the NEXT
424 complex indicated mutually exclusive binding of SF3B2 and ZCCHC8 to RBM7.
425 Thus, RBM7 appears to play dual, but not conflicting, roles during RNA processes
426 depending on its interaction with the spliceosome or exosome.

427 Currently, the pathobiological function of RBM7 in breast cancer is
428 underexplored except one study that claimed an oncogenic role of RBM7 since its
429 knockdown inhibited breast cancer cell proliferation (Xi et al., 2020). Nevertheless, in
430 our study, RBM7 knockdown in breast cancer displayed visibly pro-metastasis
431 function with activated NF-κB signaling. More importantly, according to TCGA
432 database (total cases > 1000 used for analysis), RBM7 shows decreased expression in
433 breast cancer, particularly in the metastasis loci and has positive correlation with
434 patients' survival outcomes. It is therefore highly doubtful that RBM7 could serve as
435 an oncogene in breast cancer as previously reported. Moreover, we can't exclude
436 additional biological function of RBM7 in breast cancer. RBM7-targeted silencing for
437 breast cancer would likely be detrimental for neighbouring heathy tissue and immune

438 environment as a result of NF-κB-dependent pro-inflammatory mediators and
439 cytokines secretion. Other splicing events switch triggered by RBM7 might also be
440 linked to tumor development. For example, we found RBM7 regulated alternative
441 splicing of AKT2, which is involved in glucose metabolism (Hay, 2011). Further
442 investigation is warranted to elaborate more splicing mechanisms of RBM7 in breast
443 cancer.

444 In conclusion, we discovered that down-regulated RBM7 and its cognate
445 elevated exon7-exclusion MFGE8 were tightly related to enhanced breast cancer
446 metastatic potential and poor prognosis of patients. MFGE8-L, the canonical variant,
447 possessed the capability to trigger STAT1 phosphorylation and inhibit the motility and
448 invasion of breast cancer cells, whereas splice switch to MFGE8-S was found
449 loss-of-function for this tumor-suppressive role. At another layer, RBM7 reduction led
450 to NF-κB pathway activation, resulting in enhancement of breast tumor
451 aggressiveness. Overall, our findngs implicated that activated NF-κB pathway worked
452 in concert with MFGE8 splicing transition to spur metastasis in RBM7-depleted
453 breast cancer. Additionally, although the detailed clinical significance underlying their
454 cooperation need further in-depth investigation, we propose that RBM7 and its
455 regulated splicing variants might serve as potential therapeutic biomarker and
456 prognostic indicator in breast cancer patients.

457 **Reference**

458 Anczuków O, Akerman M, Cléry A, Wu J, Shen C, Shirole Nitin H, Raimer A, Sun S, Jensen Mads A,
459 Hua Y, Allain Frédéric HT, Krainer Adrian R (2015) SRSF1-Regulated Alternative Splicing in Breast
460 Cancer. *Molecular Cell* 60: 105-117

461 Baralle D (2005) Splicing in action: assessing disease causing sequence changes. *Journal of Medical*
462 *Genetics* 42: 737-748

463 Bates SJHaDO (2008) VEGF-A splicing: the key to anti-angiogenic therapeutics? *NATURE REVIEWS*
464 7

465 Bugai A, Quaresma AJC, Friedel CC, Lenasi T, Düster R, Sibley CR, Fujinaga K, Kukanja P, Hennig T,
466 Blasius M, Geyer M, Ule J, Dölken L, Barborič M (2019) P-TEFb Activation by RBM7 Shapes a
467 Pro-survival Transcriptional Response to Genotoxic Stress. *Molecular Cell* 74: 254-267.e10

468 Chen C, Zhao S, Karnad A, Freeman JW (2018) The biology and role of CD44 in cancer progression:
469 therapeutic implications. *Journal of Hematology & Oncology* 11

470 Chen Y, Hao X, Sun R, Wei H, Tian Z (2019) Natural Killer Cell–Derived Interferon-Gamma Promotes
471 Hepatocellular Carcinoma Through the Epithelial Cell Adhesion Molecule–Epithelial-to-Mesenchymal
472 Transition Axis in Hepatitis B Virus Transgenic Mice. *Hepatology* 69: 1735-1750

473 Cheruiyot A, Li S, Nonavinkere Srivatsan S, Ahmed T, Chen Y, Lemacon DS, Li Y, Yang Z, Wadugu
474 BA, Warner WA, Pruett-Miller SM, Obeng EA, Link DC, He D, Xiao F, Wang X, Bailis JM, Walter MJ,
475 You Z (2021) Nonsense-Mediated RNA Decay Is a Unique Vulnerability of Cancer Cells Harboring
476 SF3B1 or U2AF1 Mutations. *Cancer Research* 81: 4499-4513

477 Falk S, Finogenova K, Melko M, Benda C, Lykke-Andersen S, Jensen TH, Conti E (2016) Structure of
478 the RBM7–ZCCHC8 core of the NEXT complex reveals connections to splicing factors. *Nature*

Communications 7

Feng P-C, Ke X-F, Kuang H-L, Pan L-L, Ye Q, Wu J-B (2019) RETRACTED ARTICLE: BMP2 secretion from hepatocellular carcinoma cell HepG2 enhances angiogenesis and tumor growth in endothelial cells via activation of the MAPK/p38 signaling pathway. *Stem Cell Research & Therapy* 10

Fousek K, Horn LA, Palena C (2021) Interleukin-8: A chemokine at the intersection of cancer plasticity, angiogenesis, and immune suppression. *Pharmacology & Therapeutics* 219

Fukushima K, Satoh T, Sugihara F, Sato Y, Okamoto T, Mitsui Y, Yoshio S, Li S, Nojima S, Motooka D, Nakamura S, Kida H, Standley DM, Morii E, Kanto T, Yanagita M, Matsuura Y, Nagasawa T, Kumanogoh A, Akira S (2020) Dysregulated Expression of the Nuclear Exosome Targeting Complex Component Rbm7 in Nonhematopoietic Cells Licenses the Development of Fibrosis. *Immunity* 52: 542-556.e13

Gopinathan G, Milagre C, Pearce OMT, Reynolds LE, Hodivala-Dilke K, Leinster DA, Zhong H, Hollingsworth RE, Thompson R, Whiteford JR, Balkwill F (2015) Interleukin-6 Stimulates Defective Angiogenesis. *Cancer Research* 75: 3098-3107

Harbour JW, Roberson EDO, Anbunathan H, Onken MD, Worley LA, Bowcock AM (2013) Recurrent mutations at codon 625 of the splicing factor SF3B1 in uveal melanoma. *Nature Genetics* 45: 133-135

Hay N (2011) Akt isoforms and glucose homeostasis – the leptin connection. *Trends in Endocrinology & Metabolism* 22: 66-73

Inoue D, Chew G-L, Liu B, Michel BC, Pangallo J, D'Avino AR, Hitchman T, North K, Lee SC-W, Bitner L, Block A, Moore AR, Yoshimi A, Escobar-Hoyos L, Cho H, Penson A, Lu SX, Taylor J, Chen Y, Kadoch C et al. (2019) Spliceosomal disruption of the non-canonical BAF complex in cancer. *Nature* 574: 432-436

501 Li Z, Guo Q, Zhang J, Fu Z, Wang Y, Wang T, Tang J (2021) The RNA-Binding Motif Protein Family
502 in Cancer: Friend or Foe? *Frontiers in Oncology* 11
503 Liang Y, Zhang H, Song X, Yang Q (2020) Metastatic heterogeneity of breast cancer: Molecular
504 mechanism and potential therapeutic targets. *Seminars in Cancer Biology* 60: 14-27
505 Lubas M, Andersen Peter R, Schein A, Dziembowski A, Kudla G, Jensen Torben H (2015) The Human
506 Nuclear Exosome Targeting Complex Is Loaded onto Newly Synthesized RNA to Direct Early
507 Ribonucleolysis. *Cell Reports* 10: 178-192
508 Marimuthu S, Lakshmanan I, Muniyan S, Gautam SK, Nimmakayala RK, Rauth S, Atri P, Shah A,
509 Bhyravbhatla N, Mallya K, Grandgenett PM, Hollingsworth MA, Datta K, Jain M, Ponnusamy MP,
510 Batra SK (2022) MUC16 Promotes Liver Metastasis of Pancreatic Ductal Adenocarcinoma by
511 Upregulating NRP2-Associated Cell Adhesion. *Molecular Cancer Research* 20: 1208-1221
512 Medeiros B, Allan AL (2019) Molecular Mechanisms of Breast Cancer Metastasis to the Lung: Clinical
513 and Experimental Perspectives. *International Journal of Molecular Sciences* 20
514 Meola N, Domanski M, Karadoulama E, Chen Y, Gentil C, Pultz D, Vitting-Seerup K, Lykke-Andersen
515 S, Andersen Jens S, Sandelin A, Jensen Torben H (2016) Identification of a Nuclear Exosome Decay
516 Pathway for Processed Transcripts. *Molecular Cell* 64: 520-533
517 Montes M, Sanford BL, Comiskey DF, Chandler DS (2019) RNA Splicing and Disease: Animal
518 Models to Therapies. *Trends in Genetics* 35: 68-87
519 Pascal Preker JN, Susanne Kammler, Søren Lykke-Andersen, Marianne S. Christensen, Christophe K.
520 Mapendano, Mikkel H. Schierup, Torben Heick Jensen (2008) RNA Exosome Depletion Reveals
521 Transcription Upstream of Active Human Promoters. *SCIENCE* 322: 4
522 Rabbani SA, Mazar AP (2007) Evaluating distant metastases in breast cancer: from biology to

523 outcomes. *Cancer and Metastasis Reviews* 26: 663-674

524 Raymond A, Ensslin MA, Shur BD (2009) SED1/MFG-E8: A Bi-Motif protein that orchestrates diverse

525 cellular interactions. *Journal of Cellular Biochemistry* 106: 957-966

526 Shi Y (2017) Mechanistic insights into precursor messenger RNA splicing by the spliceosome. *Nature*

527 *Reviews Molecular Cell Biology* 18: 655-670

528 Siegel RL, Miller KD, Jemal A (2019) Cancer statistics, 2019. *CA: A Cancer Journal for Clinicians* 69:

529 7-34

530 Singh RK, Cooper TA (2012) Pre-mRNA splicing in disease and therapeutics. *Trends in Molecular*

531 *Medicine* 18: 472-482

532 Smith MA, Choudhary GS, Pellagatti A, Choi K, Bolanos LC, Bhagat TD, Gordon-Mitchell S, Von

533 Ahrens D, Pradhan K, Steeples V, Kim S, Steidl U, Walter M, Fraser IDC, Kulkarni A, Salomonis N,

534 Komurov K, Boultwood J, Verma A, Starczynowski DT (2019) U2AF1 mutations induce oncogenic

535 IRAK4 isoforms and activate innate immune pathways in myeloid malignancies. *Nature Cell Biology*

536 21: 640-650

537 Tang Y, Horikawa I, Ajiro M, Robles AI, Fujita K, Mondal AM, Stauffer JK, Zheng ZM, Harris CC

538 (2012) Downregulation of splicing factor SRSF3 induces p53β, an alternatively spliced isoform of p53

539 that promotes cellular senescence. *Oncogene* 32: 2792-2798

540 Valastyan S, Weinberg Robert A (2011) Tumor Metastasis: Molecular Insights and Evolving Paradigms.

541 *Cell* 147: 275-292

542 Warzecha CC, Sato TK, Nabet B, Hogenesch JB, Carstens RP (2009) ESRP1 and ESRP2 Are Epithelial

543 Cell-Type-Specific Regulators of FGFR2 Splicing. *Molecular Cell* 33: 591-601

544 Wilkinson ME, Charenton C, Nagai K (2020) RNA Splicing by the Spliceosome. *Annual Review of*

Biochemistry 89: 359-388

Wright CJ, Smith CWJ, Jiggins CD (2022) Alternative splicing as a source of phenotypic diversity. *Nature Reviews Genetics* 23: 697-710

Xi P-W, Zhang X, Zhu L, Dai X-Y, Cheng L, Hu Y, Shi L, Wei J-F, Ding Q (2020) Oncogenic action of the exosome cofactor RBM7 by stabilization of CDK1 mRNA in breast cancer. *npj Breast Cancer* 6

Yang C, Hayashida T, Forster N, Li C, Shen D, Maheswaran S, Chen L, Anderson KS, Ellisen LW, Sgroi D, Schmidt EV (2011) The Integrin αvβ3-5 Ligand MFG-E8 Is a p63/p73 Target Gene in Triple-Negative Breast Cancers but Exhibits Suppressive Functions in ER+ and erbB2+ Breast Cancers. *Cancer Research* 71: 937-945

Zeng L, Xiao Q, Chen M, Margariti A, Martin D, Ivetic A, Xu H, Mason J, Wang W, Cockerill G, Mori K, Li JY-s, Chien S, Hu Y, Xu Q (2013) Vascular Endothelial Cell Growth–Activated XBP1 Splicing in Endothelial Cells Is Crucial for Angiogenesis. *Circulation* 127: 1712-1722

Zhou X, Wang R, Li X, Yu L, Hua D, Sun C, Shi C, Luo W, Rao C, Jiang Z, Feng Y, Wang Q, Yu S (2019) Splicing factor SRSF1 promotes gliomagenesis via oncogenic splice-switching of MYO1B. *Journal of Clinical Investigation* 129: 676-693

Zhou Z, Gong Q, Lin Z, Wang Y, Li M, Wang L, Ding H, Li P (2020) Emerging Roles of SRSF3 as a Therapeutic Target for Cancer. *Frontiers in Oncology* 10

Axel Weber PW, Michael Kracht* (2010) Interleukin-1 (IL-1) Pathway. SCIENCESIGNALING 3:105

Guo Q, Jin Y, Chen X, Ye X, Shen X, Lin M, Zeng C, Zhou T and Zhang J (2024) NF-κB in biology and targeted therapy: new insights and translational implications. Signal Transduction and Targeted Therapy 9:53

Materials and Methods

Cell culture

Human breast cancer cell lines (MDA-MB-231, MCF7, HCC1937 and BT-549) and human embryonic kidney cell HEK293T in this article were obtained from the American Type Culture Collection (ATCC). MDA-MB-231 cells were cultured without carbon dioxide at 37℃ in Leibovitz's L-15 medium (Gibco) contained 10% FBS (SINSAGE TECH). MCF7 and HEK293T cells were cultured with DMEM mediun (Gibco) supplemented with 10% FBS. HCC1937 cells were cultured with RPMI-1640 media (Gibco) supplemented with 10% FBS, while BT-549 was maintained with RPMI-1640 media (Gibco) supplemented with 10% FBS and 0.023 U/ml insulin. HUVECs were cultured with Endothelial Cell Medium (ScienCell) supplemented with ECGS (ScienCell), P/S solution (ScienCell) and 10% FBS (ScienCell). Except for MDA-MB-231, all the cells above were cultured in a 37 °C humidified incubator.

Stable breast cancer cell lines construction

To generate RBM7 overexpression vector, its coding regions (NM_016090.4) were cloned into pCDH-CMV-MCS-EF1-Puro with N-terminal Flag tag or HA-tag.To construct MFGE8-L/S vectors, the coding regions of MFGE8-L (NM_005928.4) and MFGE8-S (NM_001114614.3) were cloned into pCDH-CMV-MCS-EF1-Puro with N-terminal Flag tag. For RBM7 knockdown, target-specific shRNA (RBM7-sh1: 5'-CGAAAGGACTATGGATAACAT-3';RBM7-sh2:5'-CTACCTAGCAGATAGACA TTA-3') was cloned into pLKO.1 vector. And HEK293T cells were transfected these over-expression (or low-expression) lentivirus plasmisd together with lentivirus packaging plasmids pPAX2 and pMD2 according to the manufacturer's instructions. Viruses were collected 48 hours after transfection and then to infect breast cancer cell line with 8 ug/ml polybrene (beyotime biotechnology) for 24 hours. Positive cells were selected with 3 ug/ml puromycin.

Western Blot assay

Cells were lysed with RIPA buffer (10 mM Tris-HCl pH 7.5, 150 mM NaCl, 0.1% SDS, 1% Triton X-100, and 1% sodium deoxycholate) supplemented with protein tyrosine phosphatase inhibitor Na_3VO_4 (1mM), serine protease inhibitor PMSF (1mM) and protease inhibitor Cocktail. Immunoblotting assay was performed using standard methods. The following antibodies were used: anti-RBM7 (Sigma-Aldrich, HPA013993), anti-Flag (Sigma-Aldrich, F1804), anti-GAPDH (Proteintech, 10494-1-AP), anti-α-Tubulin (Proteintech, 11224-1-AP), anti-HA tag (Abcam, ab9110), anti-Phospho-NF-κB p65 (Cell Signaling Technology, #3033), anti-NF-κB p65 (Cell Signaling Technology, #8242), anti-IκBα (Cell Signaling Technology, #4814), anti-Phospho-IκBα (Ser32) (Cell Signaling Technology, #2859), anti-Phospho-stat1 (Tyr701) (Cell Signaling Technology, #8062), and anti-MFGE8 (R&D systems, MAB2767). The protein bands were detected with ECL enhanced chemiluminescence regent kits (NCM, Biotech), visualized using the MiniChemi™ Cheminescent image system (Beijing Sage Creation, China).

RNA isolation, RNA sequencing, and PCR

610 Total RNA from cells and tumor tissues was extracted using Trizol (Invitrogen)
611 according to the manufacturer's instructions. Total mRNA was cleaned up using
612 RNeasy Lipid Tissue Mini Kit (Qiagen, USA). And RNA-seq was carried out on
613 platform of Novogene Illumina sequencing. cDNAs were obtained using *Evo M-MLV*
614 Plus 1st Strand cDNA Synthesis Kit (Accurate Biotechnology, AG11615) with
615 random primers. qRT-PCR was carried out using MonAmp™ Universal ChemoHS
616 Specificity Plus qPCR Mix. GAPDH mRNA was examined as control for
617 normalization. Gene expression relative to GAPDH was calculated using the formula
618 $2^{-\Delta\Delta CT}$. For identified alternative splicing events, primers of the upstream and
619 downstream of variable exons or introns were designed and PCR assay was performed.
620 PCR products were subject to DNA agarose gel electrophoresis. AS events change of
621 percent-spliced-in (PSI) values were the ratio of retained splices to total transcripts.
622 The amount of each splicing isoform was measured with ImageJ. All the primers are
623 showed in Table1.

624 **Migration and invasion assays**

625 For transwell migration assay, 1×10^5 MDA-MB-231 or other breast cancer cells
626 (MCF7, BT-549 and HCC1937) were plated in the upper chamber of 6.5 mm insert
627 (Costar, USA) with 8.0 μm polycarbonate membrane with 100 μL serum-free medium.
628 For invasion assay, 1×10^5 breast cancer cells were seeded in the top chamber of each
629 Matrigel-coated insert (BD Biosciences, USA). After 24 hours or 48 hours of
630 incubation at 37 °C, migrated or invaded cells were fixed with 4% PFA and stained in
631 0.1% crystal violet. The cell number was counted by ImageJ software in 3 views from
632 3 independent experiments.

633 **Wound healing**

634 Knockdown RBM7 in MDA-MB-231 and 4T1 cells or control cells were implanted
635 into 6-well culture dishes. When the cells grew about 90% confluence, lines of the
636 same width were drawn on the bottom of the culture dish using autoclaved sterile tips.
637 Images were captured at 0 and 36 hours after the wounding. Data shown were
638 representative of three independent repeats.

639 **Gelatin Degradation Assay**

640 To evaluate the ability of breast cancer cells to form invadopodia and degrade matrix,
641 QCM Gelatin Invadopodia Assay (ECM670-1, Merck Millipore) was performed
642 according to the manufacturers' protocol. Briefly, 1×10^4 MFGE8-L/S-overexpressing
643 or control MDA-MB-231 cells were suspended in L-15 medium with 10% FBS and
644 seeded into the pre-treated 96-well plate. After 48 hours, the cells were washed twice
645 with PBS. Fix cells with 3.7% formaldehyde for 30 minutes. Then these cells were
646 stained respectively with TRITC-phalloidin and DAPI for 1 hour. The ability of cells
647 to degrade the matrix was imaged using immunofluorescence microscopy (LEICA
648 DMi8, Germany) and the area of invadopodia was measured using the Image J
649 software.

650 **Tube formation of HUVECs assay**

651 Capillary tube formation assay was used to observe angiogenesis of HUVECs.
652 HUVECs were seeded into 48-well plate coated with growth factor reduced Matrigel
653 (BD Biosciences). HUVECs cells were treated with conditioned medium for 4-5

654 hours and then formation of capillary-like tubes was observed and stained with
655 calcein for 30 minutes. Images of blood vessels were taken using fluorescence
656 microscopy. And the tube length was analyzed by ImageJ software.

657 **Immunofluorescence assay**

658 After seeded on coverslips for 36 hours, the MDA-MB-231 cells were immersion
659 fixed with 4% PFA for 20 minutes at room temperature, washed 3 times in PBS. Then
660 the cells were treated with 0.2 % Triton-X100 in PBS for 10 minutes and blocked with
661 3% BSA for 10 minutes. Next the cells were immersed in primary antibody at 4℃
662 overnight, washed in PBS 3 times for 5 minutes each, and incubated with secondary
663 antibody labelled with Alexa fluorophore 488/592 for 1 hour at RT. After washing 3
664 times in PBS, the cells were dyed with DAPI. In addition, antibodies targeting RBM7
665 (Sigma, HPA013993), and Flag (Sigma, 3165) were used in the assay. The pictures
666 are captured with fluorescent microscope (Leica, USA).

667 **RNA immunoprecipitation assay**

668 RNA immunoprecipitation was performed as previously described. In brief,
669 HEK293T cells were transfected Flag-RBM7 or control plasmid. After 48 hours of
670 transfection, Flag-RBM7 or control cells were collected and cross-linked by 1%
671 formaldehyde, homogenized in lysis buffer (50 mM Tris-HCl Ph 7.5, 0.4 M NaCl, 1
672 mM EDTA, 1mM DTT, 0.5% TritonX-100, 10% Glycerol supplemented with RNase
673 inhibitor and broad-spectrum protease inhibitors Cocktail), and broke with an
674 ultrasonic crusher. And solubilized cell lysate was obtained and precleared by
675 ProteinG-agarose beads together with nonspecific tRNA to remove nonspecific
676 binding. Then binding RNAs with RBM7 protein were precipitated with Anti-Flag
677 M2 Affinity beads. Co-precipitated RNAs were subject to RT-PCR. Input controls
678 (total RNAs) and Flag-controls were assayed simultaneously to prove that the
679 detected signals were the result of RNAs specifically binding to RBM7. The
680 gene-specific primers were designed MFGE8-RIP1-F:5'-tatttatgccccctcaccgc-3';
681 MFGE8-RIP1-R:5'-atggtggctgcctgtaat-3';MFGE8-RIP2-F:5'-ctgaggctcacccaagtag-3';
682 MFGE8-RIP2-R:5'-GTAGGATGCCACAAACTG-3'). GAPDH mRNA was as
683 negative control (GAPDH-F 5'-GGGGAAGGTGAAGGTCG-G-3'; GAPDH-R
684 5'-TTGAGGTCAATGAAGGGG-3').

685 **Antisense oligonucleotide (ASO)-mediated splicing blockade**

686 MFGE8-ASOs were synthesized with a full-length phosphorothioate backbone and
687 2'-O-methyl modified ribose molecules (GenScriptBiotech Corp). ASO was
688 transfected at final concentration of 500 nM using Lipofectamine3000 (Thermo Fisher
689 Scientific) according to the manufacturer's instructions. The MCF7 cells were
690 harvested for RNA and splicing assays 48 h after transfection.

691 **Animal experiments**

692 All procedures and experimental protocols involving mice were approved by the
693 Institutional Animal Care and Use Committee (IACUC) of Dalian Medical University
694 (approval no. AEE21015). Female BALB/C mice (6 weeks old, 4-5 mice per group as
695 indicated in figures and/or figure legends) were injected into tail vein with murine
696 4T1 breast cancer cells (6×10^5 cells) to develop mice model of pulmonary metastasis.
697 After about 3 weeks, all mice were euthanized, and lungs were harvested, fixed and

paraffin embedded. After lungs were H&E stained, the number of metastatic lesions were enumerated by pathologist using brightfield microscopy.

Clinical tissues samples collection

All human breast cancer tissues or normal tissue were obtained with written informed consent from patients or their guardians prior to participation in the study. The Institutional Review Board of the Dalian Medical University approved use of the tumor specimens in this study (approval no.PJ-KS-KY-2022-208).

Bioinformatics analysis

RBM7 expression data and survival data (including OS and DFS) were obtained from the METABRIC database using the Cbioportal web tool. Based on the expression level of RBM7, the patients were divided into four categories (i.e., Q1, Q2, Q3, Q4) by quartiles, and then log-rank was employed to compare the survival differences of patients in different categories. Cbioportal cited (Cerami E et al. The cBio cancer genomics portal: an open platform for exploring multidimensional cancer genomics data. Cancer Discov. 2012 May;2(5):401-4). Through the analysis of alternative splicing events in RBM7 knocked-down MDA-MB-231 cells compared to control, exon skipping events were screened out, and then selected the sequence of the 500nt region upstream of the alternative exon for subsequent base sequence enrichment analysis. The XSTREME tool provided by the online tool meme-suite (https://meme-suite.org/meme/) was used to perform Motif Discovery and Enrichment Analysis. E-value < 0.05 as the significance standard to output the results.

Statistical analyses

Statistical analyses and statistical graphs were conducted by GraphPad Prism 8 software. To compare the differences between the two variables, Student's T-test, one-way ANOVA with Dunnett multiple comparisons, and one-way ANOVA with Tukey's multiple comparisons according to the specific situation were applied. $*P < 0.05$, $**P < 0.01$, $***P < 0.001$, and $****P < 0.0001$ indicated the significant difference.

Data availability

The authors declare that all the data supporting the findings of this study are available within the article and its supplementary information files. RNA-seq data in this study have been deposited in Gene Expression Omnibus of NCBI with the accession code GSE248938.

Acknowledgements

This work was supported by the National Key R&D Program of China (2022YFA1104002, 2023YFE0117500 to YW); the National Natural Science Foundation of China (82225034, 81830088 to YW; 82103148 to YQ; 81872247 to WZ); the Science and Technology Innovation Foundation of Dalian (2022JJ11CG009

to YW), Liaoning Revitalization Talents Program (XLYC2202027 to YW); Interdisciplinary Research Cooperation Project Team Funding of Dalian Medical University (JCHZ2023008 to YQ); Joint Research Program of Natural Science Foundation of Liaoning, China (2023-MSLH-023 to YQ); the Science and Technology Innovation Talent Support Program of Dalian (2022RQ056 YQ); Dalian High Level Talents Renovation Supporting Program (2019RQ097 to WZ).

Study Approval

The Institutional Animal Care and Use Committee of the Dalian Medical University approved use of animal models in this study (approval no. AEE21015). All human tumor tissues were obtained with written informed consent from patients or their guardians prior to participation in the study. The Institutional Review Board of of the First Affiliated Hospital of Dalian Medical University approved use the tumor specimens in this study (approval no. PJ-KS-KY-2022-208).

750 **Figure legends**

751 **Figure 1. Decreased RBM7 expression was associated with poor prognosis of**
752 **breast cancer.** (A-B) The correlation between RBM7 mRNA expression and overall
753 survival (OS) or disease-free-survival (DFS) of breast cancer patients (n=1980) was
754 analyzed based on the METABRIC dataset. The samples were divided into four equal
755 parts, containing lower quartile Q1, median quartile Q2, upper quartile Q3 and higher
756 quartile Q4 according to the expression of RBM7. Data are presented as means ± SD
757 and *P* values were obtained by Mantel-Cox log-rank test. (C) The expression of
758 RBM7 in primary breast carcinoma (n=1097) compared to normal tissues (n=114)
759 was analyzed through UALCAN dataset. (D) Analysis of RBM7 expression in breast
760 cancer lymph node metastases in comparison with breast cancer tissues with no lymph
761 node metastasis based on TCGA dataset. BRCA samples were classified into N0 (No
762 regional lymph node involvement) (n=515), and metastases in lymph node (N1-N3)
763 (n=565). (E) Representative IHC images of RBM7 staining for patients at high (n=32)
764 or low (n=58) clinical stages on tissue microarray of breast cancer specimens. Scale
765 bars = 300 μm (top) or 30 μm (bottom). (F) Representative images of the IHC staining
766 of RBM7 in a tissue microarray containing triple-negative breast cancer (n=119) and
767 para-carcinoma tissues (n=20). Scale bars = 300 μm (top) and 30 μm (bottom). (G)
768 Quantitative analysis of RBM7 expression according to IHC staining scores in
769 primary breast cancer (n=12) and distant metastases (breast cancer lung metastases,
770 n=4; breast cancer liver metastases, n=5). (H-I) Representative IHC images and
771 quantitative analyses for RBM7 staining in 3 paired primary breast cancer and
772 lymphatic metastases are shown. Scale bar = 100 μm. Data are presented as means ±
773 SD and *P* values were obtained by unpaired Student t test (C-I). $^{**}P < 0.01$, $^{***}P <$
774 0.001, $^{****}P < 0.0001$.

775 **Figure 2. RBM7 negatively regulated breast cancer metastatic potential.** (A)
776 Gene Ontology analysis showed the significantly affected biological process upon
777 RBM7 knockdown in MDA-MB-231 cells. (B) Functional association network of
778 RBM7-regulated targets. The genes were analyzed using the STRING database, and
779 subgroups are marked according to their function. (C) A heatmap showing the

780 qRT-PCR analysis of differentially expressed genes upon RBM7 knockdown in breast
781 cancer cells from three biological replicates. (D-F) 4T1 cells without or with RBM7
782 knockdown were injected into tail vein of immunodeficient BALB/c mice to establish
783 a lung metastasis model. Spontaneous pulmonary metastases were assessed after
784 about 3 weeks, the white arrow indicates lung lesions macroscopically (D). H&E
785 stained lung sections were quantified for the number of spontaneous metastatic
786 lesions from BALB/c mice (n=6, 5 and 9). Data are presented as mean ± SD and *P*
787 values were determined by one-way ANOVA with Dunnett's multiple comparisons
788 test (E). Representative images of H&E stained lung sections are shown. Top panel
789 scale bars indicate 7 mm; bottom panel scale bars indicate 300 μm (F) . (G-J) The
790 metastatic ability of breast cancer cells with RBM7 depletion (G) or ectopic
791 expression of RBM7 (I) were evaluated by transwell assay. Scale bars: 100 μm. Data
792 are mean ± SD from three random fields. *P* values were determined by one-way
793 ANOVA with Dunnett's multiple comparisons test (H) or unpaired Student's T test (J).
794 (K) Representative images of the tube formation of HUVEC cells treated with
795 conditional medium from RBM7-KD cells or control cells for 12h. Scale bars: 100
796 μm. Quantification of number of junctions formed by HUVEC was calculated by
797 Image J software. $^{**}P < 0.01$, $^{***}P < 0.001$, $^{****}P < 0.0001$.

798 **Figure 3. Global identification of alternative splicing events regulated by RBM7.**
799 (A-E) RNA-seq analysis was performed on RBM7-knockdown MDA-MB-231 cells
800 or control cells, and the changes in splicing events were analyzed. (A) Volcano plot
801 illustrating up-regulated/down-regulated alternative splicing events upon RBM7
802 depletion. (B) Comparison of the differential splicing events in five types of AS
803 events affected by RBM7 depletion. (C) The relative fraction of splicing events
804 undergoing percent spliced in (PSI) increase or decrease induced by RBM7 depletion.
805 (D) Alternative splicing of MFGE8 was chosen to represent a decrease of PSI, and
806 numbers of exon junction reads were indicated. (E) The hit top enriched motifs
807 identified in the differential spliced genes regulated by RBM7. (F) RBM7-regulated
808 exon skipping events were identified by semiquantitative RT-PCR using
809 RBM7-depleted or control MDA-MB-231 cells (see also Figure 3-source data 1/

810 source data 2). The mean ± SD of PSI from 3 independent experiments was plotted,
811 with *P* values determined by one-way ANOVA with Dunnett's multiple comparisons
812 test. (G) Gene Ontology analysis showed the significantly enriched biological
813 processes of changed splicing events affected upon RBM7 knockdown in
814 MDA-MB-231 cells. (H) KEGG pathway enrichment analysis of functional
815 association network of the RBM7-controlled AS targets.

816 **Figure 4. RBM7 knockdown promoted exon 7 skipping of MFGE8.** (A)
817 Comparison of RBM7-binding candidates from the RNA immunoprecipitation (RIP)
818 sequencing (GSE144075 dataset) and two gene sets containing top 43 differentially
819 AS genes in RNA-seq data of breast cancer cells expressing RBM7 shRNA1/2 as
820 presented by venn diagram. The gene lists on the right were shown according to the
821 FDR *P* value of top genes with significantly changed AS in RNA-seq. (B) Upper:
822 schematics of human MFGE8 pre-mRNA (NM_005928.4). MFGE8-long isoform
823 included the exon 7 (hereafter referred to as MFGE8-L), whereas it is skipped in
824 MFGE8-short isoform (hereafter referred to as MFGE8-S). The arrow indicates the
825 direction of transcription. Lower: primers were designed on exon 6/8, and RT-PCR
826 was performed to identify PSI changes using RBM7-knockdown or control
827 MDA-MB-231 cells. The base peak diagram of sanger sequencing of RT-PCR results
828 showed the splicing junction sites (filled with gray). (C) Various breast cancer cells
829 lines with stable depletion of RBM7 or control were constructed. Alternative splicing
830 events of MFGE8 regulated by RBM7 were examined by semi-quantitative RT-PCR.
831 The knockdown efficiency of RBM7 expression was detected by Western Blotting.
832 (see also Figure 4-source data 1/ source data 2). The mean ± SD of PSIs from three
833 independent repeated experiments were plotted with *P* value calculated by one-way
834 ANOVA with Dunnett's multiple comparisons test. (D) Left, Schematics of MFGE8
835 mini-splicing reporter including exons 6-8 and two flanking introns in the 600bp
836 region upstream and downstream of 5'/3' splice sites; middle, RBM7 stable
837 knockdown or control cells were transfected with splicing reporter and collected for
838 RNA extraction after 48h. The splicing changes of exogenous MFGE8 were detected
839 by RT-PCR with specific primers on the reporter gene. The level of RBM7 protein

840 was detected in MCF7 cells by western blotting (see also Figure 4-source data 3/
841 source data 4). *P* value was calculated by one-way ANOVA with Dunnett's multiple
842 comparisons test from three repeated experiments. (E) As shown in schematic
843 diagram, orange box indicates cassette exon 7 and primers were designed in the
844 putative binding regions P1 and P2. Binding of MFGE8 pre-mRNA with RBM7 was
845 examined by RIP assay in HEK293T cells expressing Flag-RBM7. (see also Figure
846 4-source data 5/ source data 6) (F) Upper: the red line in diagram indicates ASOs
847 targeting region which contain UUUCUU residues; down: MCF7 and BT-549 cells
848 were transfected with ASOs targeting MFGE8 pre-mRNA for 48h and then applied
849 for RT-PCR identification (see also Figure 4-source data 7/ source data 8). *$P < 0.05$,
850 **$P < 0.01$, ***$P < 0.001$, and ****$P < 0.0001$.

851 **Figure 5. MFGE8-L inhibited breast cancer cell migration and invasion.** (A) The
852 function of MFGE8-L/S on breast cancer cell migration and invasion were evaluated
853 by transwell assays. (B) Gelatin degradation assay was performed to test the effect of
854 RBM7 knockdown on invadopodia function. 10000 cells were plated onto
855 FITC-gelatin substrates (Green) and cultured for 48 h. Representative images are
856 shown (red, Cy3-phalloidin; blue, DAPI) and the degraded areas were quantified by
857 Image J software. Scar bars= 50 μm. *P* values were determined by one-way ANOVA
858 with Tukey's multiple comparisons test (n = 3). (C) The subcellular localizations of
859 MFGE8 isoforms. MDA-MB-231 cells were transfected with Flag-tagged MFGE8-L
860 or MFGE8-S, and visualized with immunofluorescence assay. Scale bar = 10 μm. The
861 percent of cells with foci were quantified and plotted (about 80 cells were captured
862 and quantified in both samples). (D-E) The KEGG pathway and Gene ontology
863 analysis of genes up-regulated by MFGE-S compared with MFGE8-L. (F) The
864 expression levels of p-STAT1(Tyr701) in HCC1937 cells overexpressing MFGE8-L/S
865 was detected by western blotting. (see also Figure 5-source data 1/ source data 2). *P*
866 values were determined by one-way ANOVA with Tukey's multiple comparisons test.
867 **$P < 0.01$, ****$P < 0.0001$.

868 **Figure 6. RBM7 knockdown enhanced aggressiveness of breast cancer relying on**
869 **MFGE8 splicing switch to the short variant and NF-κB pathway activation.** (A)

870 Breast cancer cells MDA-MB-231 and MCF7 were cotransfected with shRNA
871 targeting RBM7 or control and shRNA-resistant Flag-MFGE8-L vectors and then
872 subjected to transwell migration assay or invasion assay. Migrated or invaded cells
873 were counted from random sites of the transwell with Image J. *P* values were
874 determined by one-way ANOVA with Tukey's multiple comparison test. (B)
875 Representative transwell analysis of migrative/invasive capability of breast cancer
876 cells transfected with 500 nM ASO directed against RBM7-binding region in MFGE8
877 pre-mRNA. Cells migrating through transwell membrane with matrigel or not were
878 imaged and representative images are shown (upper) along with quantification (down).
879 *P* values were determined by one-way ANOVA with Tukey's multiple comparison test.
880 (C) The expression of metastasis-related factors in HCC1937 and BT-549 cells stably
881 expressing MFGE8-L, MFGE8-S or control vector was measured by real-time PCR
882 assay. (D) NF-κB signaling pathway was enrichment via KEGG analysis in RBM7
883 knockdown breast cancer cells. (E) Western blotting showed the expression of p65,
884 p-p65, IκBα and p-IκBα in NF-κB pathway in RBM7-depleted or control
885 MDA-MB-231 and BT-549 breast cancer cells (see also Figure 6-source data 1/
886 source data 2). (F) Western blotting was performed to test the expression of RBM7,
887 p65 and p-p65 in RBM7-depleted MDA-MB-231 cells treated with or without NF-κB
888 inhibitor PDTC 10 μm for 48h (see also Figure 6-source data 3/ source data 4). (G)
889 Representative images of the tube formation of HUVEC cells treated with conditional
890 medium from RBM7-depleted MDA-MB-231 in the presence or absence of 10 μm
891 NF-κB inhibitor PDTC. Scale bars: 100 μm. Quantification of junctions of endothelial
892 network was conducted by ImageJ software. *P* values were determined by one-way
893 ANOVA with Tukey's multiple comparison test (n = 3). $*P < 0.05$, $**P < 0.01$,
894 $***P < 0.001$, and $****P < 0.0001$.

895 **Figure 7. Splicing shift of MFGE8 toward exon7 exclusion was negatively**
896 **correlated with RBM7 expression in patients with breast cancer.** (A) MFGE8
897 exon7 expression level was analyzed in breast carcinoma in comparison with normal
898 tissues based on the TCGA dataset. Plotted are the mean ± SD from 114 normal

899 tissues and 1094 tumor tissues, with **** $P<0.0001$ as determined by unpaired
900 Student' t test. (B) The splicing alteration of MFGE8 in 6 pairs of primary breast
901 cancer tissues and adjacent normal tissues was examined using RT-PCR (see also
902 Figure 7-source data 1/ source data 2). The quantification of PSI vales was based on
903 relative band intensities using Image J software. (C) The splicing alteration of
904 MFGE8 in primary breast cancer tissues and corresponding lymph node metastases
905 was identified by RT-PCR assays (see also Figure 7-source data 3/ source data 4). The
906 quantification of PSI vales was determined by Image J software. (D) The correlation
907 between the expression of MFGE8 exon7 and overall survival (OS) of breast cancer
908 patients was analyzed based on the TCGA dataset. *P* value was assessed with
909 Mantel-Cox log-rank test. (E) Correlation of RBM7 expression with MFGE8 exon7
910 levels was analyzed using Pearson's correlation coefficient method. (F) The
911 mechanistic model of how RBM7 regulated metastasis of breast cancer through
912 regulating MFGE8 splicing switch.

913 **Figure 1-figure supplement 1. The low expression of RBM7 in breast cancer was**
914 **positively correlated with poor prognosis of breast cancer patients.** (A) The
915 correlation between RBM7 expression and overall survival of breast cancer patients
916 based on data from the Kaplan–Meier Plotter cohort. (B-C) METABRIC analysis of
917 the correlation between RBM7 expression and overall survival (OS) or disease-free
918 survival (DFS) of breast cancer patients based on the METABRIC dataset. *P* value
919 was obtained by log-rank test (A, B, C). (D) RBM7 mRNA level was analyzed in
920 breast invasive carcinoma based on lymph nodal metastasis status from the UALCAN
921 dataset. *P* value was calculated by unpaired Student's t-test by comparing different
922 types of lymph node metastasis of breast cancer with normal tissue (n=114). N,
923 Lymph node metastases: N0, no metastases (n=516); N1, 1 – 3 metastases (n=362);
924 N2, 4 – 9 metastases (n=120); N3, 10 or more metastases (n=77).

925 **Figure 2-figure supplement 1. RBM7 depletion promoted breast cancer cell**
926 **migration and invasion.** (A) The mouse cell line 4T1 with RBM7 knockdown was
927 constructed. The knockdown efficiency of RBM7 was detected by real-time
928 quantitative PCR. (B) The migration and invasion ability of RBM7-knockdown 4T1

929 cells was detected by transwell chambers coated with or without Matrigel. (C) The
930 metastatic capability of RBM7-depleted 4T1 cells was evaluated by wound healing
931 assay. (D) Western blotting showed the expression of RBM7 in MDA-MB-231 and
932 MCF7 cells with RBM7 depletion (see also Figure 2-figure supplementary 1-source
933 data 1/ source data 2). (E) The metastatic capability of RBM7 on MDA-MB-231 cells
934 was evaluated by wound healing assay. (F) Western blotting showed the expression of
935 RBM7 in various breast cancer cell lines with ectopic expression of RBM7 (see also
936 Figure 2-figure supplementary 1-source data 3/ source data 4). (G) The metastatic
937 ability of BT-549 cells and HCC1937 cells upon RBM7 overexpression was evaluated
938 by transwell assay. Data are mean ± SD from three random fields. *P* values were
939 determined by unpaired Student's T test (G). *P* value was calculated by one-way
940 ANOVA with Dunnett's multiple comparisons test (A, B, C, E).

941 **Figure 3-figure supplement 1. RBM7 had a potential role in regulating**
942 **alternative splicing of breast cancer cells.** (A) Immunofluoresence shows
943 endogenous RBM7 subcellular localization in breast cancer cell lines. (B)
944 Semi-quantitative RT-PCR was performed to validate the RI (intron retention) and
945 A5E (alternative 5' splice site exon) splicing events in MDA-MB-231 cells with
946 RBM7 knockdown compared with vector control (see also Figure 3-figure
947 supplementary 1-source data 1/ source data 2). *P* value was calculated by one-way
948 ANOVA with Dunnett's multiple comparisons test. (C) MFGE8 min-splicing
949 reporters with mutation in the RBM7 binding site or a non-specific binding were
950 generated and shown in cartoon (left); RT-PCR assays were performed to identify the
951 splicing outcomes of MFGE8 reporter while RBM7 was depleted in breast cancer
952 cells (right). See also Figure 3-figure supplementary 1-source data 3/ source data 4.

953 **Figure 5-figure supplement 1. MFGE8-L suppressed breast cancer cells**
954 **migration and invasion.** (A) The protein expression of MFGE8 was determined by
955 western blot in MDA-MB-231 cells with over-expression or knockdown of MFGE8-L.
956 SE denotes long exposure and LE denotes long exposure (see also Figure 5-figure
957 supplementary 1-source data 1/ source data 2). (B-C) Transwell assay with Matrigel
958 or not was performed using MDA-MB-231 cells with overexpression (B) or depletion

959 (C) of MFGE8. *P* value was calculated by unpaired Student's t test. (D) Western blot
960 showed the extrinsic expression of MFGE8-L or MFGE8-S isoform in MDAMB-231
961 and HCC1937 transfected with Flag-MFGE8-L, Flag-MFGE8-S or empty vectors
962 respectively (see also Figure 5-figure supplementary 1-source data 3/ source data 4).
963 The red arrow indicates the position of MFGE8-L/S protein band . (E) MDA-MB-231
964 cell line over-expressing MFGE8-L, MFGE8-S or vector control were analyzed by
965 wound healing assay. The scratch healing rates were measured in triplicate
966 experiments with mean ± SD plotted (*P* values were calculated by one-way ANOVA
967 with Tukey's multiple comparisons test). (F) Schematic diagram of the domain
968 composition of two MFGE8 isoforms. Upper: the full-length variant with exon7
969 indicated by yellow square; down: the truncated variant with exon7 skipping. (G) The
970 model structure of two MFGE8 isoforms was implemented using SwissModel
971 software. The F5/8 type C2 protein domain excluded from MFGE8-S variant was
972 marked in red. (H) Transcriptome sequencing was performed using MDA-MB-231
973 cells overexpressing MFGE8-L or MFGE8-S. Venn diagram of 782 MFGE8-L
974 down-regulated genes compared to control and 647 MFGE8-S up-regulated genes
975 compared to MFGE8-L.

976 **Figure 6-figure supplement 1. MFGE8-L/S isoforms had no effect on NF-κB**
977 **pathway in breast cancer cells.** (A) MCF7 and MDA-MB-231 cells stably
978 expressing shRNA against RBM7 with ectopic MFGE8-L or control vector were
979 generated. The expression of RBM7 and MFGE8 was measured by qRT-PCR assay.
980 (B) RT-PCR quantification of two MFGE8 isoforms after transfecting breast cancer
981 cells with 500 nM ASO directed against RBM7-binding region in MFGE8 pre-mRNA.
982 See also Figure 6-figure supplementary 1-source data 1/ source data 2. (C) HCC1937
983 and BT-549 cells stably expressing MFGE8-L, MFGE8-S or control were generated.
984 The expression of MFGE8 was measured by qRT-PCR assay. (D) Representative
985 images of the tube formation of HUVEC cells treated with conditional medium from
986 breasst cancer cells with ectopic expression of MFGE8-L or MFGE8-S for 48h. Scale
987 bars: 100 μm. Quantification of number of junctions formed by HUVEC was

988 determined by Image J software. (E) Western blotting results showed the
989 phosphorylation and expression of p65 in RBM7-overexpressing breast cancer cells
990 (see also Figure 6-figure supplementary 1-source data 3/ source data 4). (F) Western
991 blotting was performed to detect the indicated proteins in breast cancer cells with
992 up-expression of MFGE8-L/S (see also Figure 6-figure supplementary 1-source data
993 5/ source data 6). (G) The mRNA levels of IL-1β in MDA-MB-231 or BT549 cells
994 with stable RBM7 knockdown or control vector were examined by qRT-PCR
995 approach. (H) Supernatants from RBM7-knockdown MDA-MB-231 or BT549 cells
996 were collected and protein expression of IL-1β was measured by ELISA kit. (I) The
997 knockdown efficiency of RBM7 in two breast cancer cell lines were determined by
998 qRT-PCR approach. (J) RBM7-depleted MDA-MB-231 cells were treated with or
999 without NF-κB inhibitor PDTC 10 μm for 48h. Then Transwell assays were
1000 performed to assess cell migration ability. *P* values were calculated by one-way
1001 ANOVA with Tukey's multiple comparisons.
1002 **Figure 7-figure supplement 1. MFGE8 exon7 skipping is enhanced in a variety of**
1003 **cancers.** (A) The PSI values for the MFGE8 exon7 were analyzed in various cancers
1004 according to TCGA SpliceSeq dataset. *P* value was calculated by unpaired Student's
1005 t-test. (B) Immunoprecipitation assay was performed in breast cancer cells expressing
1006 HA-RBM7 and Flag-SF3B2 or empty vector. The Flag-tagged precipitated complexes
1007 and lysates were analyzed through western blotting. See also Figure 7-figure
1008 supplementary 1-source data 1/ source data 2. (C) The splicing shift of MFGE8 upon
1009 SF3B2 knockdown in breast cancer cells was examined by RT-PCR approach. See
1010 also Figure 7-figure supplementary 1-source data 3/ source data 4. The mean ± SD of
1011 PSI values derived from three independent replicates is shown. (D) The SF3B2
1012 knockdown efficiency was examined by qRT-PCR assays. *P* value was calculated by
1013 unpaired Student's t-test.
1014
1015
1016
1017

1018 **Legends for source data**

1019 Figure 3—source data 1

1020 Original file for the RT-PCR analysis of splicing shifts in Figure 3F (MFGE8, AKT2,
1021 ZMYN8 or MBNL1).

1022 Figure 3—source data 2

1023 PDF containing Figure 3F and original scans of the relevant RT-PCR analysis of
1024 splicing shifts (MFGE8, AKT2, ZMYN8 or MBNL1) with highlighted bands and
1025 sample labels.

1026 Figure 4—source data 1

1027 Original file for the RT-PCR analysis of MFGE8 splicing switch and Western blot
1028 identification of RBM7 knockdown in various breast cancer cell lines in Figure 4C.

1029 Figure 4—source data 2

1030 PDF containing Figure 4C and original scans of the relevant RT-PCR analysis for
1031 MFGE8 splicing switch and Western blot identification of RBM7 knockdown with
1032 highlighted bands and sample labels.

1033 Figure 4—source data 3

1034 Original file for the RT-PCR analysis of splicing switch in MFGE8 mini-splicing
1035 reporter and Western blot identification of RBM7 knockdown in Figure 4D.

1036 Figure 4—source data 4

1037 PDF containing Figure 4D and original scans of the relevant RT-PCR analysis of
1038 splicing switch in MFGE8 mini-splicing reporter and Western blot identification of
1039 RBM7 knockdown with highlighted bands and sample labels.

1040 Figure 4—source data 5

1041 Original file for the RT-PCR analysis of RBM7 protein- MFGE8 pre-mRNA binding
1042 from RIP assay in Figure 4E.

1043 Figure 4—source data 6

1044 PDF containing Figure 4E and original scans of the RT-PCR analysis of RBM7

1045 protein- MFGE8 pre-mRNA binding from RIP assay with highlighted bands and
1046 sample labels.

1047 Figure 4—source data 7

1048 Original file for the RT-PCR analysis of MFGE8 splicing switch upon ASO treatment
1049 in Figure 4F.

1050 Figure 4—source data 8

1051 PDF containing Figure 4F and original scans of the relevant RT-PCR analysis for
1052 splicing switch of MFGE8 variants with highlighted bands and sample labels.

1053 Figure 5—source data 1

1054 Original file for the Western blot analysis in Figure 5F (anti-P-STAT1, anti-MFGE8
1055 and anti-GAPDH).

1056 Figure 5—source data 2

1057 PDF containing Figure 5F and original scans of the relevant Western blot analysis
1058 (anti-P-STAT1, anti-MFGE8 and anti-GAPDH) with highlighted bands and sample
1059 labels.

1060 Figure 6—source data 1

1061 Original file for the Western blot analysis in Figure 6E (anti-p65, anti-P-p65, anti-IκB,
1062 anti-P-IκB, anti-RBM7 and anti-GAPDH).

1063 Figure 6—source data 2

1064 PDF containing Figure 6E and original scans of the relevant Western blot analysis
1065 (anti-p65, anti-P-p65, anti-IκB, anti-P-IκB, anti-RBM7 and anti-GAPDH)) with
1066 highlighted bands and sample labels.

1067 Figure 6—source data 3

1068 Original file for the Western blot analysis in Figure 6F (anti-p65, anti-P-p65,
1069 anti-RBM7 and anti-GAPDH)).

1070 Figure 6—source data 4

1071 PDF containing Figure 6F and original scans of the relevant Western blot analysis

1072 (anti-p65, anti-P-p65, anti-RBM7 and anti-GAPDH)) with highlighted bands and
1073 sample labels.

1074 Figure 7—source data 1

1075 Original file for the RT-PCR analysis of MFGE8 splicing switch in primary breast
1076 cancer tissues and adjacent normal tissues in Figure 7B.

1077 Figure 7—source data 2

1078 PDF containing Figure 7B and original scans of the relevant RT-PCR analysis for
1079 MFGE8 splicing switch with highlighted bands and sample labels in primary breast
1080 cancer tissues and adjacent normal tissues .

1081 Figure 7—source data 3

1082 Original file for the RT-PCR analysis of MFGE8 splicing switch in primary breast
1083 cancer tissues and corresponding lymph node metastases in Figure 7C.

1084 Figure 7—source data 4

1085 PDF containing Figure 7C and original scans of the relevant RT-PCR analysis for
1086 splicing switch of MFGE8 variants with highlighted bands and sample labels in
1087 primary breast cancer tissues and corresponding lymph node metastases.

1088

1089 Figure 2-figure supplement 1—source data 1

1090 Original file for the Western blot analysis in Figure 2-figure supplement 1D
1091 (anti-RBM7 and anti-tubulin).

1092 Figure 2-figure supplement 1—source data 2

1093 PDF containing Figure 2-figure supplement 1D and original scans of the relevant
1094 Western blot analysis (anti-RBM7 and anti-tubulin) with highlighted bands and
1095 sample labels.

1096 Figure 2-figure supplement 1—source data 3

1097 Original file for the Western blot analysis in Figure 2-figure supplement 1F
1098 (anti-RBM7 and anti-tubulin).

1099 Figure 2-figure supplement 1—source data 4

1100 PDF containing Figure 2-figure supplement 1F and original scans of the relevant
1101 Western blot analysis (anti-RBM7 and anti-tubulin) with highlighted bands and
1102 sample labels.

1103 Figure 3-figure supplement 1—source data 1

1104 Original file for the RT-PCR analysis of MAP7D1 or HNRNPC splicing switch in
1105 Figure 3-figure supplement 1B.

1106 Figure 3-figure supplement 1—source data 2

1107 PDF containing Figure 3-figure supplement 1B and original scans of the relevant
1108 RT-PCR analysis for splicing switch of MAP7D1 or HNRNPC variants with
1109 highlighted bands and sample labels.

1110 Figure 3-figure supplement 1—source data 3

1111 Original file for RT-PCR analysis of splicing switch of MFGE8 minigene reporter in
1112 Figure 3-figure supplement 1C.

1113 Figure 3-figure supplement 1—source data 4

1114 PDF containing Figure 3-figure supplement 1C and original scans of the relevant
1115 RT-PCR analysis of MFGE8 splicing switch with highlighted bands and sample
1116 labels.

1117 Figure 5-figure supplement 1—source data 1

1118 Original file for the Western blot analysis in Figure 5-figure supplement 1A
1119 (anti-MFGE8 and anti-GAPDH).

1120 Figure 5-figure supplement 1—source data 2

1121 PDF containing Figure 5-figure supplement 1A and original scans of the relevant
1122 Western blot analysis (anti-MFGE8 and anti-GAPDH) with highlighted bands and
1123 sample labels.

1124 Figure 5-figure supplement 1—source data 3

1125 Original file for the Western blot analysis in Figure 5-figure supplement 1D (anti-Flag

1126 and anti-GAPDH).

1127 Figure 5-figure supplement 1—source data 4

1128 PDF containing Figure 5-figure supplement 1D and original scans of the relevant
1129 Western blot analysis (anti-Flag and anti-GAPDH) with highlighted bands and sample
1130 labels.

1131 Figure 6-figure supplement 1—source data 1

1132 Original file for the RT-PCR analysis of MFGE8 splicing switch upon ASO treatment
1133 in Figure 6-figure supplement 1B.

1134 Figure 6-figure supplement 1—source data 2

1135 PDF containing Figure 6-figure supplement 1B and original scans of the relevant
1136 RT-PCR analysis for splicing switch of MFGE8 variants with highlighted bands and
1137 sample labels.

1138 Figure 6-figure supplement 1—source data 3

1139 Original file for the Western blot analysis in Figure 6-figure supplement 1E (anti-p65,
1140 anti-P-p65, anti-IκB, anti-P-IκB, anti-Flag and anti-GAPDH).

1141 Figure 6-figure supplement 1—source data 4

1142 PDF containing Figure 6-figure supplement 1E and original scans of the relevant
1143 Western blot analysis (anti-p65, anti-P-p65, anti-IκB, anti-P-IκB, anti-Flag and
1144 anti-GAPDH)) with highlighted bands and sample labels.

1145 Figure 6-figure supplement 1—source data 5

1146 Original file for the Western blot analysis in Figure 6-figure supplement 1F (anti-p65,
1147 anti-P-p65, anti-RBM7 and anti-GAPDH)).

1148 Figure 6-figure supplement 1—source data 6

1149 PDF containing Figure 6-figure supplement 1F and original scans of the relevant
1150 Western blot analysis (anti-p65, anti-P-p65, anti-RBM7 and anti-GAPDH)) with
1151 highlighted bands and sample labels.

1152 Figure 7-figure supplement 1—source data 1

1153 Original file for the Western blot analysis of Flag-tagged precipitated complexes in
1154 Figure 7-figure supplement 1B (anti-Flag, anti-HA and anti-GAPDH).

1155 Figure 7-figure supplement 1—source data 2

1156 PDF containing Figure 7-figure supplement 1B and original scans of the relevant
1157 Western blot analysis of Flag-tagged precipitated complexes (anti-Flag, anti-HA and
1158 anti-GAPDH) with highlighted bands and sample labels.

1159 Figure 7-figure supplement 1—source data 3

1160 Original file for RT-PCR analysis of splicing switch of MFGE8 upon SF3B2
1161 knockdown in Figure 7-figure supplement 1C.

1162 Figure 7-figure supplement 1—source data 4

1163 PDF containing Figure 7-figure supplement 1C and original scans of the relevant
1164 RT-PCR analysis of MFGE8 splicing switch upon SF3B2 knockdown with
1165 highlighted bands and sample labels.

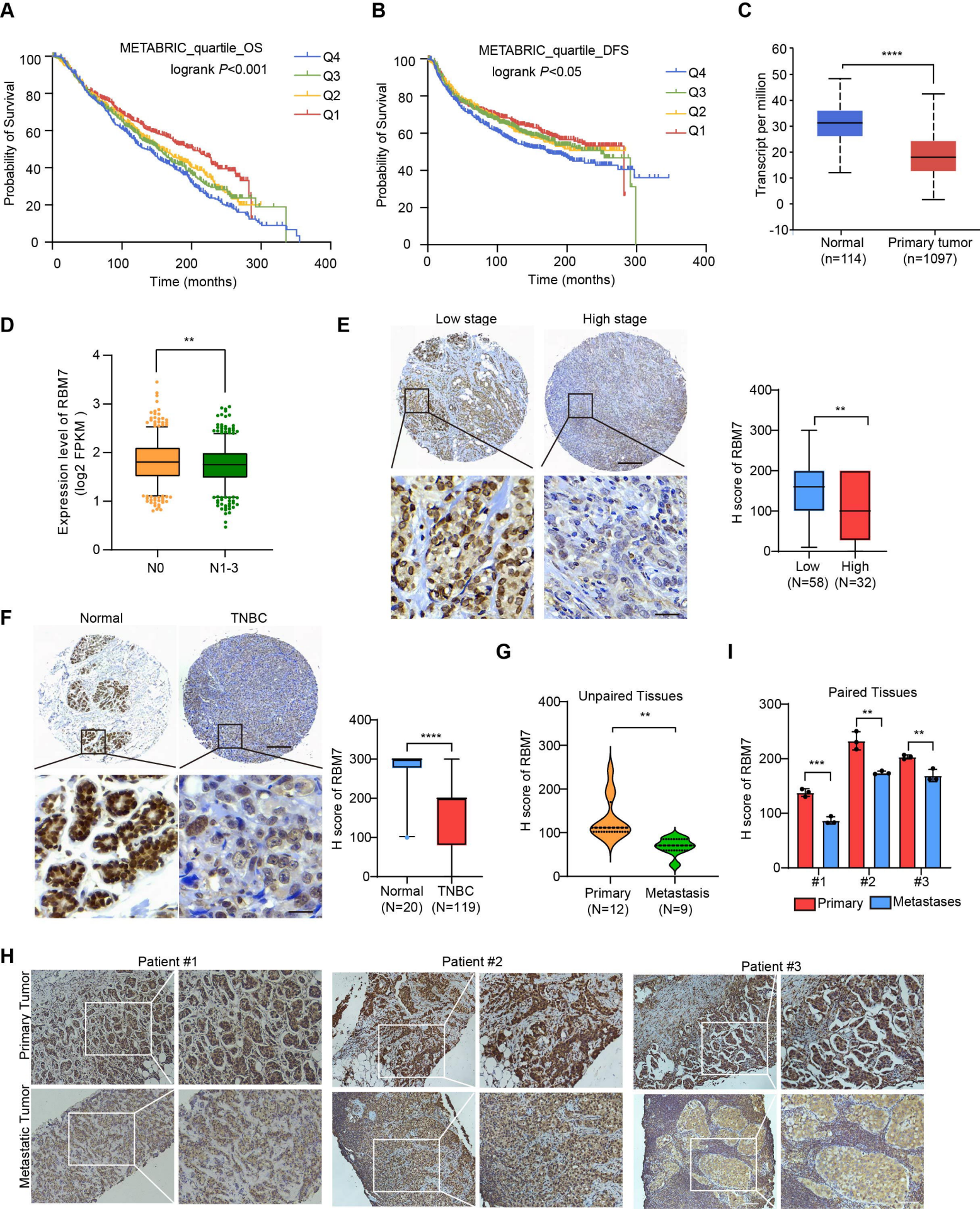
A
METABRIC_quartile_OS
logrank P<0.001
Q4
Q3
Q2
Q1
Probability of Survival
Time (months)
B
METABRIC_quartile_DFS
logrank P<0.05
Q4
Q3
Q2
Q1
Probability of Survival
Time (months)
C
****
Transcript per million
Normal (n=114)
Primary tumor (n=1097)
D
**
Expression level of RBM7 (log2 FPKM)
N0
N1-3
E
Low stage
High stage
**
H score of RBM7
Low (N=58)
High (N=32)
F
Normal
TNBC
****
H score of RBM7
Normal (N=20)
TNBC (N=119)
G
Unpaired Tissues
**
H score of RBM7
Primary (N=12)
Metastasis (N=9)
I
Paired Tissues
***
**
**
H score of RBM7
#1
#2
#3
Primary
Metastases
H
Patient #1
Patient #2
Patient #3
Primary Tumor
Metastatic Tumor

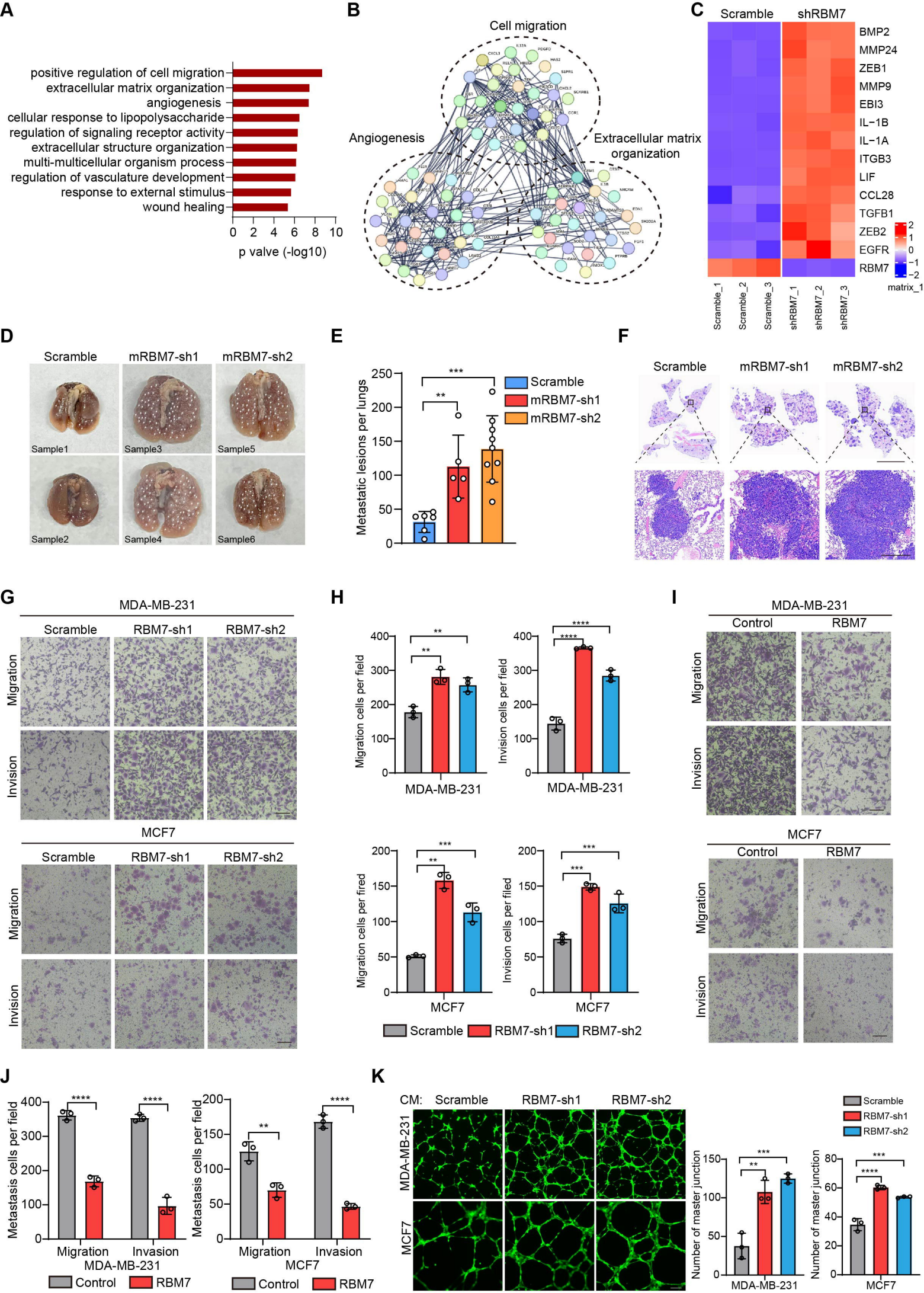
A
positive regulation of cell migration
extracellular matrix organization
angiogenesis
cellular response to lipopolysaccharide
regulation of signaling receptor activity
extracellular structure organization
multi-multicellular organism process
regulation of vasculature development
response to external stimulus
wound healing
0 2 4 6 8 10
p valve (-log10)
B
Cell migration
Angiogenesis
Extracellular matrix organization
C
Scramble
shRBM7
BMP2
MMP24
ZEB1
MMP9
EBI3
IL−1B
IL−1A
ITGB3
LIF
CCL28
TGFB1
ZEB2
EGFR
RBM7
Scramble_1
Scramble_2
Scramble_3
shRBM7_1
shRBM7_2
shRBM7_3
matrix_1
D
Scramble
mRBM7-sh1
mRBM7-sh2
Sample1
Sample3
Sample5
Sample2
Sample4
Sample6
E
Metastatic lesions per lungs
Scramble
mRBM7-sh1
mRBM7-sh2
F
Scramble
mRBM7-sh1
mRBM7-sh2
G
MDA-MB-231
Scramble
RBM7-sh1
RBM7-sh2
Migration
Invision
MCF7
H
Migration cells per field
Invision cells per field
MDA-MB-231
Migration cells per fired
Invision cells per filed
MCF7
Scramble
RBM7-sh1
RBM7-sh2
I
MDA-MB-231
Control
RBM7
Migration
Invision
MCF7
J
Metastasis cells per field
Migration
Invasion
MDA-MB-231
MCF7
Control
RBM7
K
CM:
Scramble
RBM7-sh1
RBM7-sh2
MDA-MB-231
MCF7
Number of master junction

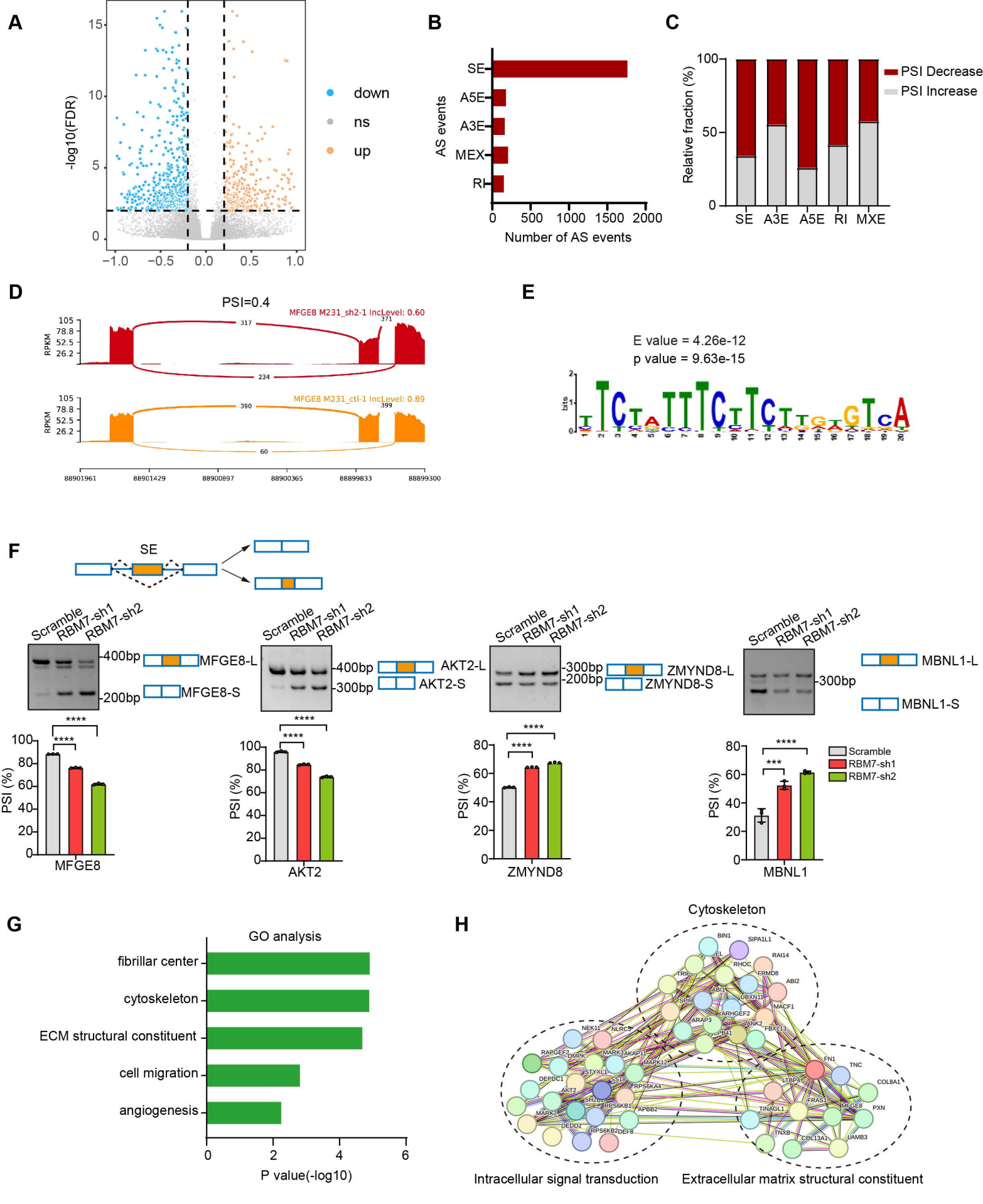
A
-log10(FDR)
down
ns
up
B
AS events
SE
A5E
A3E
MEX
RI
Number of AS events
C
Relative fraction (%)
PSI Decrease
PSI Increase
SE
A3E
A5E
RI
MXE
D
PSI=0.4
MFGE8 M231_sh2-1 IncLevel: 0.60
MFGE8 M231_ctl-1 IncLevel: 0.89
RPKM
E
E value = 4.26e-12
p value = 9.63e-15
bits
F
SE
Scramble
RBM7-sh1
RBM7-sh2
MFGE8-L
MFGE8-S
AKT2-L
AKT2-S
ZMYND8-L
ZMYND8-S
MBNL1-L
MBNL1-S
PSI (%)
MFGE8
AKT2
ZMYND8
MBNL1
G
GO analysis
fibrillar center
cytoskeleton
ECM structural constituent
cell migration
angiogenesis
P value(-log10)
H
Cytoskeleton
Intracellular signal transduction
Extracellular matrix structural constituent

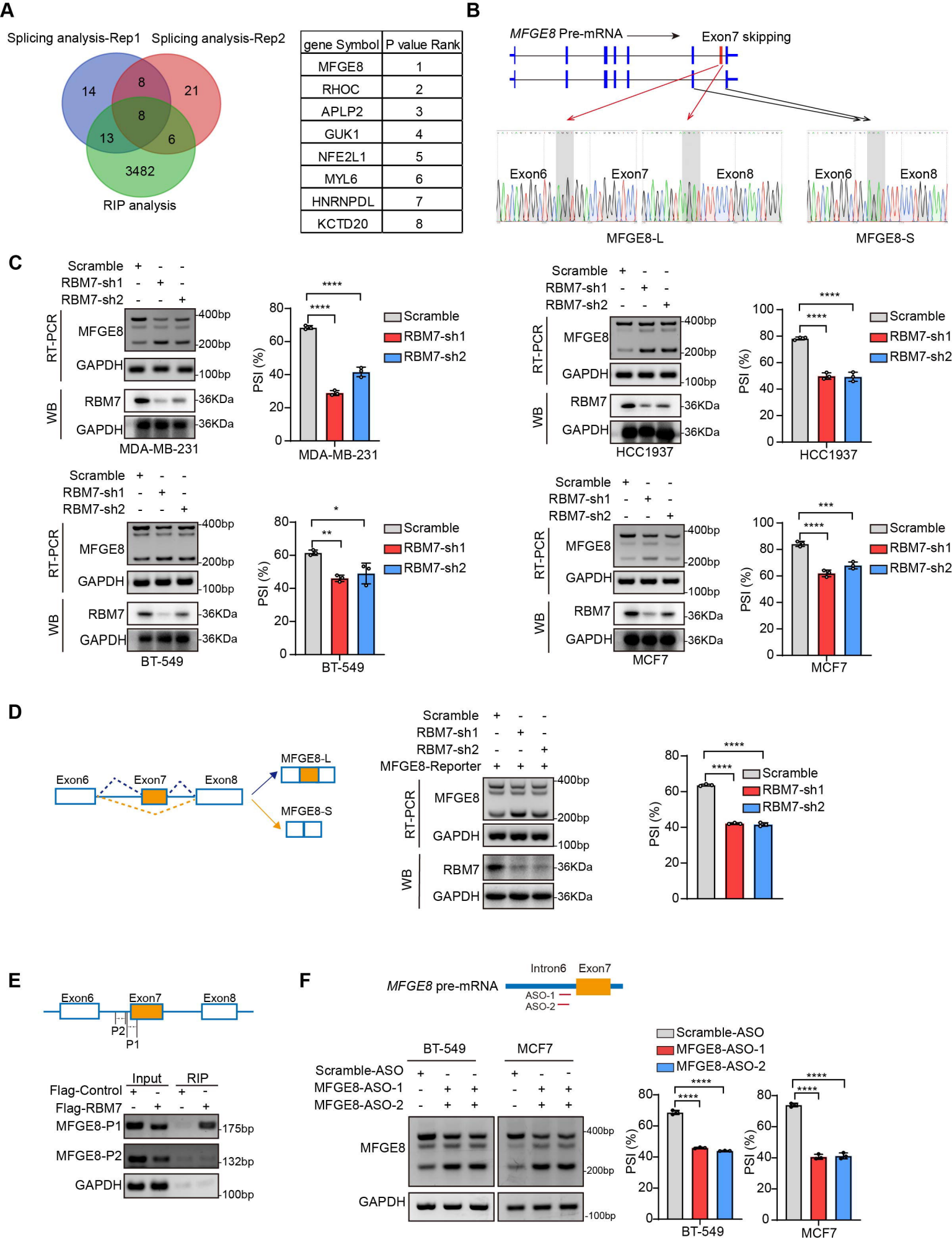
A
Splicing analysis-Rep1
Splicing analysis-Rep2
14
8
21
8
13
6
3482
RIP analysis
gene Symbol | P value Rank
MFGE8 | 1
RHOC | 2
APLP2 | 3
GUK1 | 4
NFE2L1 | 5
MYL6 | 6
HNRNPDL | 7
KCTD20 | 8
B
MFGE8 Pre-mRNA
Exon7 skipping
Exon6
Exon7
Exon8
MFGE8-L
MFGE8-S
C
Scramble
RBM7-sh1
RBM7-sh2
RT-PCR
WB
MFGE8
GAPDH
RBM7
400bp
200bp
100bp
36KDa
MDA-MB-231
HCC1937
BT-549
MCF7
PSI (%)
D
Exon6
Exon7
Exon8
MFGE8-L
MFGE8-S
MFGE8-Reporter
E
P2
P1
Input
RIP
Flag-Control
Flag-RBM7
MFGE8-P1
MFGE8-P2
175bp
132bp
F
Intron6
Exon7
ASO-1
ASO-2
Scramble-ASO
MFGE8-ASO-1
MFGE8-ASO-2

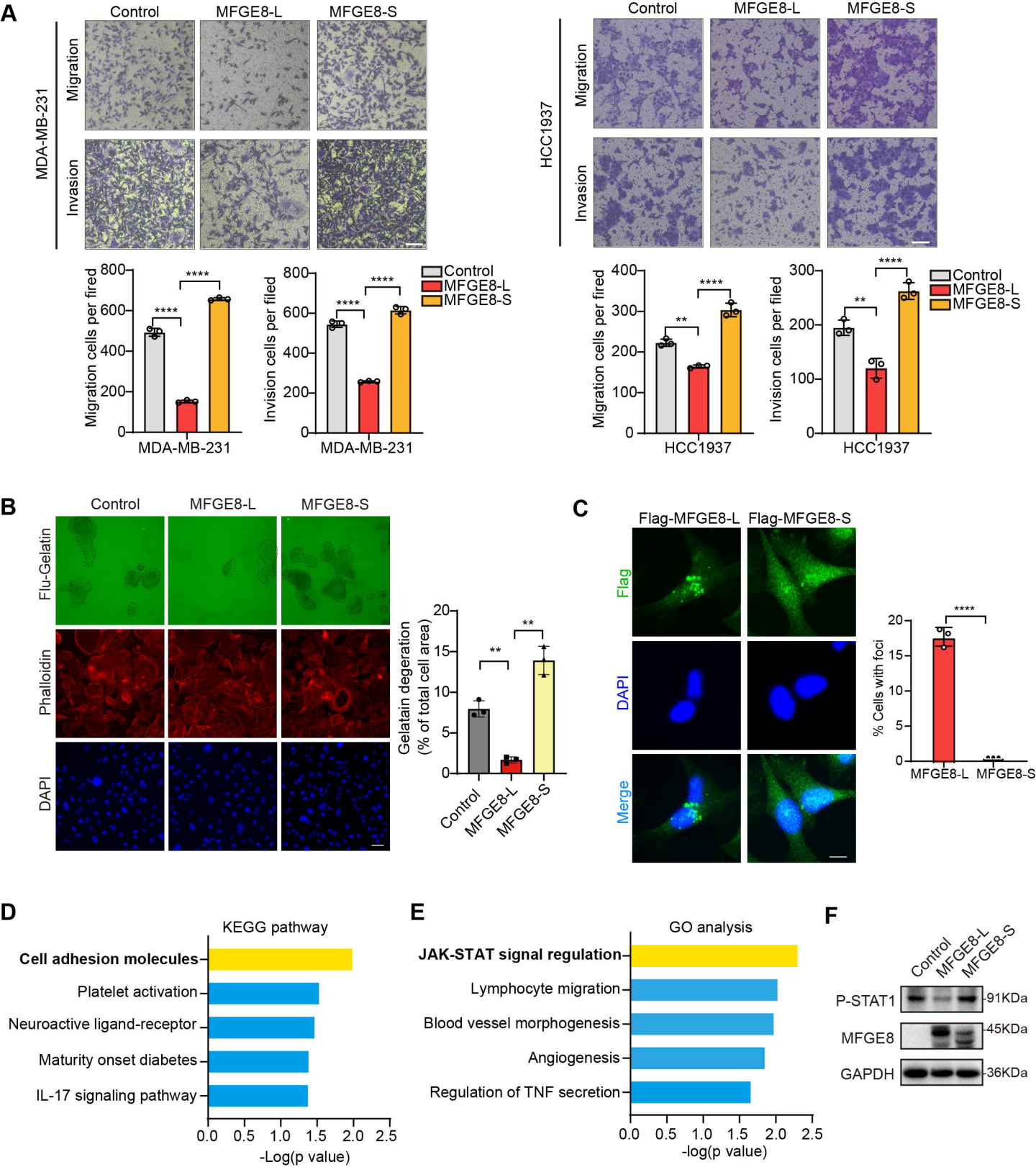
A
Control
MFGE8-L
MFGE8-S
MDA-MB-231
Migration
Invasion
HCC1937
Migration cells per fired
Invision cells per filed
MDA-MB-231
HCC1937
Control
MFGE8-L
MFGE8-S
B
Flu-Gelatin
Phalloidin
DAPI
Gelatain degeration (% of total cell area)
C
Flag-MFGE8-L
Flag-MFGE8-S
Flag
DAPI
Merge
% Cells with foci
D
KEGG pathway
Cell adhesion molecules
Platelet activation
Neuroactive ligand-receptor
Maturity onset diabetes
IL-17 signaling pathway
-Log(p value)
E
GO analysis
JAK-STAT signal regulation
Lymphocyte migration
Blood vessel morphogenesis
Angiogenesis
Regulation of TNF secretion
-log(p value)
F
P-STAT1
MFGE8
GAPDH
91KDa
45KDa
36KDa

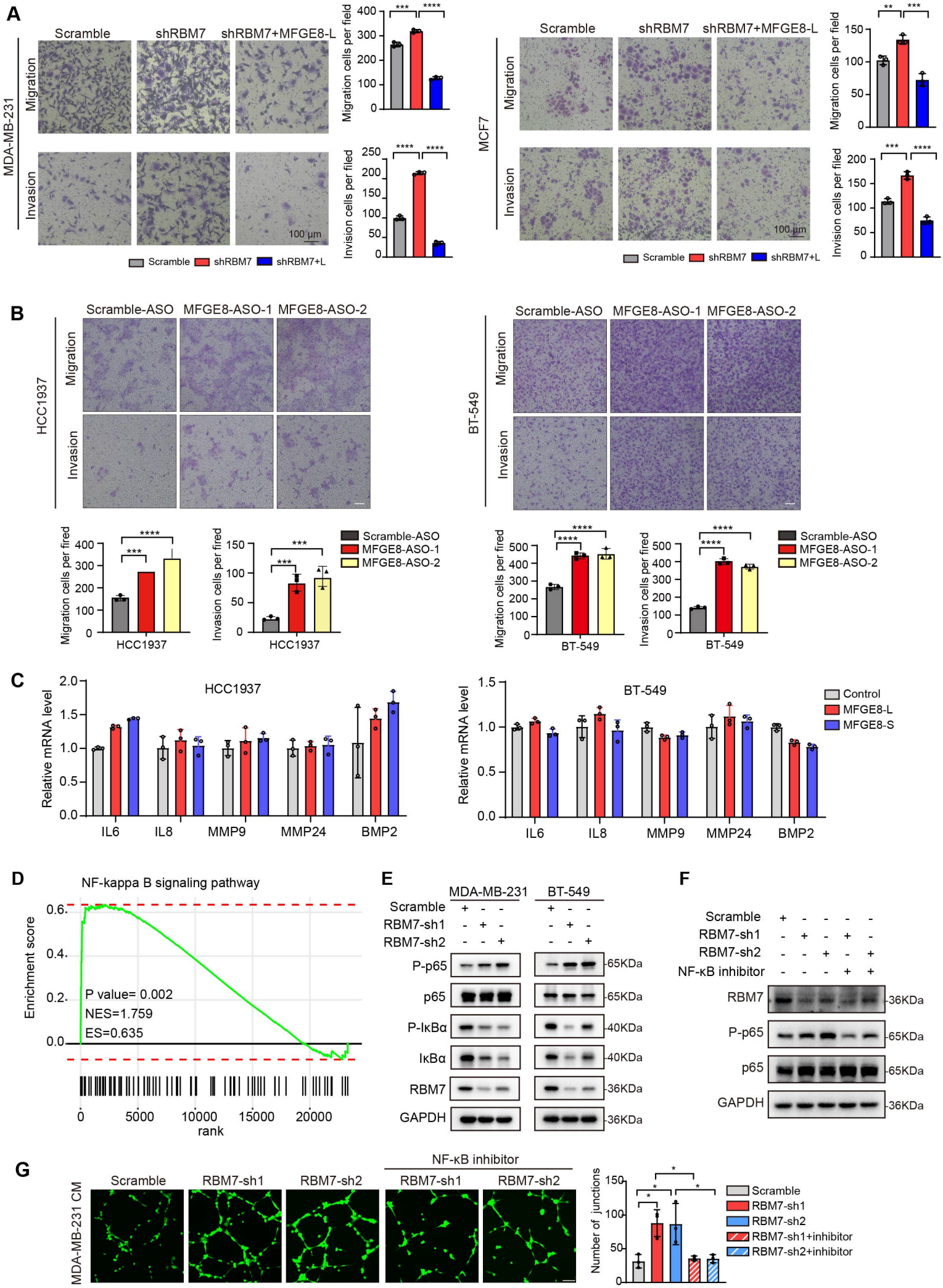
A
Scramble
shRBM7
shRBM7+MFGE8-L
MDA-MB-231
Migration
Invasion
100 μm
Migration cells per field
Invision cells per filed
Scramble
shRBM7
shRBM7+L
MCF7
B
Scramble-ASO
MFGE8-ASO-1
MFGE8-ASO-2
HCC1937
BT-549
Migration cells per fired
Invasion cells per fired
C
HCC1937
BT-549
Relative mRNA level
IL6
IL8
MMP9
MMP24
BMP2
Control
MFGE8-L
MFGE8-S
D
NF-kappa B signaling pathway
Enrichment score
P value= 0.002
NES=1.759
ES=0.635
rank
E
MDA-MB-231
BT-549
Scramble
RBM7-sh1
RBM7-sh2
P-p65
p65
P-IκBα
IκBα
RBM7
GAPDH
65KDa
40KDa
36KDa
F
NF-κB inhibitor
G
MDA-MB-231 CM
Number of junctions
RBM7-sh1+inhibitor
RBM7-sh2+inhibitor

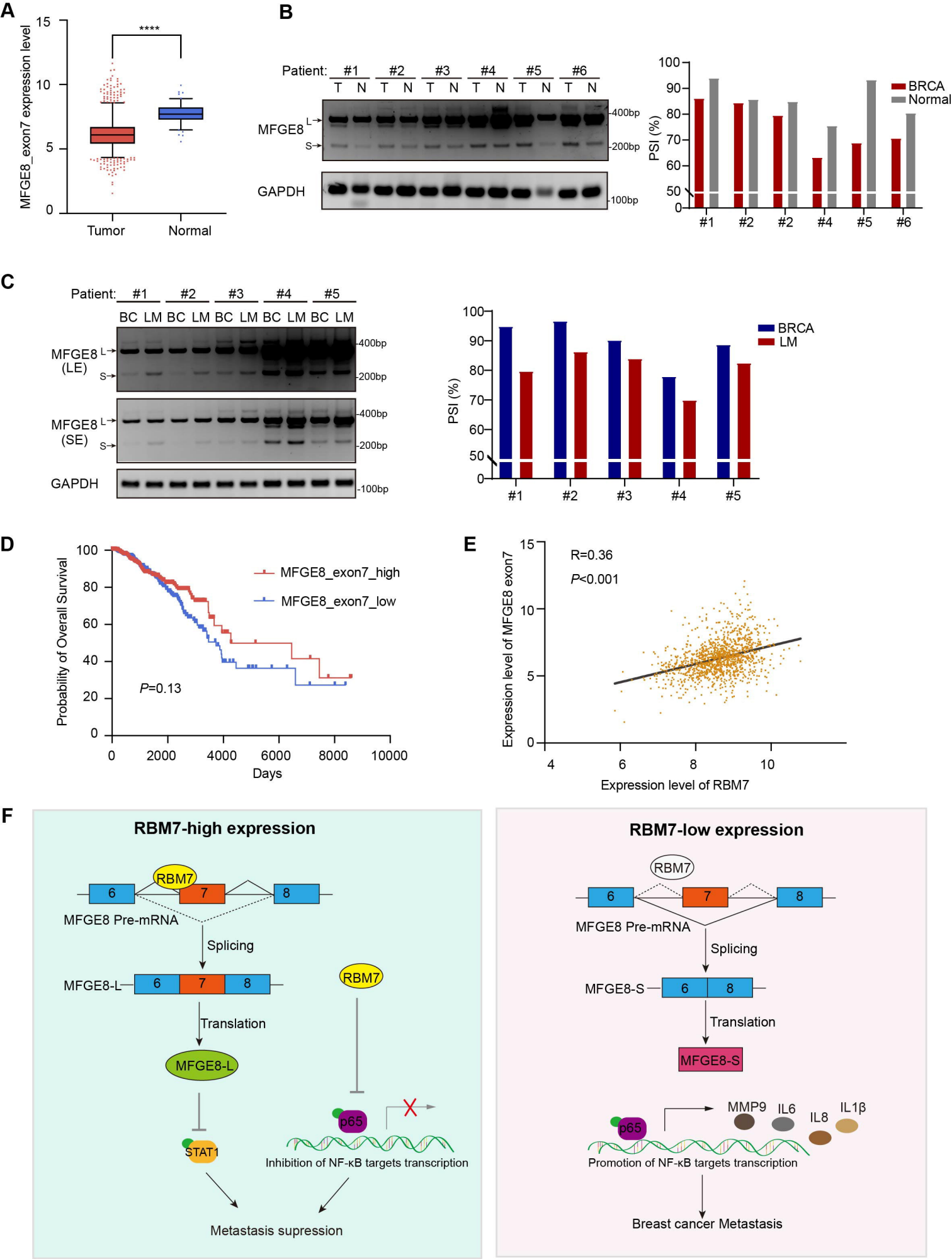
A
MFGE8_exon7 expression level
****
Tumor
Normal
B
Patient: #1 #2 #3 #4 #5 #6
T N T N T N T N T N T N
MFGE8 L
S
GAPDH
400bp
200bp
100bp
PSI (%)
BRCA
Normal
C
Patient: #1 #2 #3 #4 #5
BC LM BC LM BC LM BC LM BC LM
MFGE8 (LE)
MFGE8 (SE)
GAPDH
BRCA
LM
D
Probability of Overall Survival
MFGE8_exon7_high
MFGE8_exon7_low
P=0.13
Days
E
R=0.36
P<0.001
Expression level of MFGE8 exon7
Expression level of RBM7
F
RBM7-high expression
RBM7
MFGE8 Pre-mRNA
Splicing
MFGE8-L
Translation
MFGE8-L
STAT1
p65
Inhibition of NF-κB targets transcription
Metastasis supression
RBM7-low expression
RBM7
MFGE8 Pre-mRNA
Splicing
MFGE8-S
Translation
MFGE8-S
p65
MMP9
IL6
IL8
IL1β
Promotion of NF-κB targets transcription
Breast cancer Metastasis